Journal of Low Temperature Physics, Vol. 140, Nos. 1/2, July 2005 (© 2005)
DOI: 10.1007/s10909-005-6016-3

Magnetic Quantum Tunneling in the Single-Molecule Magnet Mn_{12}-Acetate

E. del Barco,[1,*] A. D. Kent,[1] S. Hill,[2] J. M. North,[3] N. S. Dalal,[3] E. M. Rumberger,[4] D. N. Hendrickson,[4] N. Chakov,[5] and G. Christou[5]

[1]*Department of Physics, New York University, 4 Washington Place, New York, NY 10003, USA*
E-mail: andy.kent@nyu.edu
[2]*Department of Physics, University of Florida, Gainsville, FL 32611-8440, USA*
E-mail: Hill@phys.uf1.edu
[3]*Department of Chemistry and Biochemistry and National High Magnetic Field Laboratory, Florida State University, Tallahassee, FL 32606, USA*
[4]*Department of Chemistry and Biochemistry, University of California San Diego – La Jolla, CA 92093-0358, USA*
[5]*Department of Chemistry, University of Florida, Gainsville, FL 32611-7200, USA*

(Received January 7, 2005; revised February 16, 2005)

The symmetry of magnetic quantum tunneling (MQT) in the single molecule magnet Mn_{12}-acetate has been determined by sensitive low-temperature magnetic measurements in the pure quantum tunneling regime and high frequency EPR spectroscopy in the presence of large transverse magnetic fields. The combined data set definitely establishes the transverse anisotropy terms responsible for the low temperature quantum dynamics. MQT is due to a disorder induced locally varying quadratic transverse anisotropy associated with rhombic distortions in the molecular environment (2nd order in the spin-operators). This is superimposed on a 4th order transverse magnetic anisotropy consistent with the global (average) S_4 molecule site symmetry. These forms of the transverse anisotropy are incommensurate, leading to a complex interplay between local and global symmetries, the consequences of which are analyzed in detail. The resulting model explains: (1) the observation of a twofold symmetry of MQT as a function of the angle of the transverse magnetic field when a subset of molecules in a single crystal are studied; (2) the non-monotonic dependence of the tunneling probability on the magnitude of the transverse magnetic field, which is ascribed to an interference (Berry phase)effect; and (3) the angular dependence of

*Present address: Department of Physics, University of Central Florida, Orlando, FL 32816-2385, USA. E-mail: delbarco@physics.ucf.edu

0022-2291/05/0700-0119/0

EPR absorption peaks, including the fine structure in the peaks, among many other phenomena. This work also establishes the magnitude of the 2nd and 4th order transverse anisotropy terms for Mn_{12}-acetate single crystals and the angle between the hard magnetic anisotropy axes of these terms. EPR as a function of the angle of the field with respect to the easy axes (close to the hard-medium plane) confirms that there are discrete tilts of the molecular magnetic easy axis from the global (average) easy axis of a crystal, also associated with solvent disorder. The latter observation provides a very plausible explanation for the lack of MQT selection rules, which has been a puzzle for many years.

KEY WORDS: single-molecule magnet, quantum tunneling, molecular nanomagnet, Mn_{12}-Acetate, EPR, magnetometry

1. INTRODUCTION

The origin of magnetic quantum tunneling (MQT) in single-molecule magnets (SMMs) is important for fundamental reasons as well as proposed applications, ranging from magnetic data storage to quantum computing.[1,2] A macroscopic (millimeter-sized) SMM single crystal to a first approximation can be considered an ensemble of weakly interacting molecules with the same chemical composition and orientation. In this regard SMM single crystals are ideal materials in which to study the quantum properties of magnetic molecules, as the magnetic response is amplified by the huge number of molecules forming the crystal. The environment of the molecules in crystals is also well defined and can be characterized by techniques such as **x**-ray diffraction.

SMMs have a predominant uniaxial magnetic anisotropy that determines an easy magnetic axis for the spin. MQT is due to interactions that break this axial symmetry and lead to transitions between magnetic states with opposite projections of spin on the magnetic easy axis. While this is fundamental to their quantum dynamics, remarkably only recently have the nature of the transverse interactions that produce MQT been determined in the first and most studied SMM, Mn_{12}-acetate (henceforth Mn_{12}-ac).[3–19] Small modulations in the local environment around the magnetic cores have been found to be important in MQT.[16–19] In particular, it has been shown that in Mn_{12}-ac there are a variety of types of disorder that affect the magnetic properties of the molecules, including a distribution of solvent microenvironments, leading to g- and D-strain[20–26] and a distribution of tilts of the easy axes of the molecules.[27,28]

In this paper, we present high sensitivity magnetometry and high frequency electron paramagnetic resonance (EPR) studies carried out on single crystals of Mn_{12}-ac. These experimental techniques and an in-depth

analysis of the implications of the combined data set allow us to determine the symmetry and origin of MQT. We show that variations in the local solvent environments around the $Mn_{12}O_{12}$ magnetic cores are important to MQT because they lower the symmetry of the core and lead to tilts of the magnetic easy axis. Disorder in the molecules' solvent environment can explain many of the features observed experimentally. This includes non exponential magnetic relaxation, the absence of tunneling selection rules, an unusual Berry phase effect, and multiple and broad EPR absorption peaks.

The article is organized as follows: In Sec. 2 we analyze the spin Hamiltonian of Mn_{12}-ac and discuss the symmetry of MQT expected based on this Hamiltonian. The effect of a disorder induced transverse anisotropy combined with intrinsic transverse anisotropy has interesting consequences for MQT that we explore in depth. In Sec. 3 we describe magnetic relaxation measurements carried out in the pure quantum regime, where the MQT is not assisted by thermal activation.[11] Sec. 4 presents high frequency EPR measurements. In Sec. 5, we discuss the implications of our analysis and measurements to the understanding of MQT.

2. TUNNELING IN Mn_{12}-AC

Mn_{12}-ac consist of a core of four Mn^{+4} ions (S = 3/2) surrounded by a ring of eight Mn^{+3} ions (spin S = 2) (see Fig. 1). These two groups of spins order ferrimagnetically producing a net spin $S = 10 (8 \times 2 - 4 \times 3/2 = 10)$.[29–31]

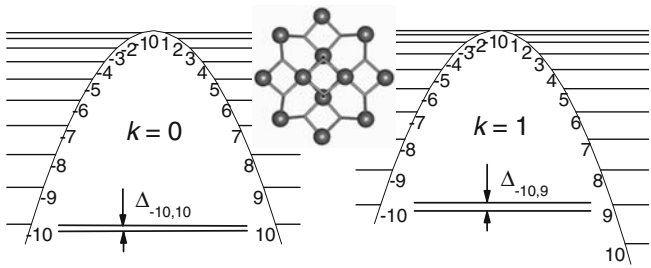

Fig. 1. Energy diagram of the $2S+1=21$ projections of the spin $S=10$ along the easy magnetic axis of the Mn_{12}-ac molecule for resonances $k=0$ and $k=1$ (note k=m+m′). The tunnel splitting, $\Delta_{m,m'}$, is illustrated in both cases (not to scale). The inset shows the arrangement of Mn ions looking down the S_4 axis of the molecule (z-axis). Note that the spins point up and down along this axis, perpendicular to the plane of the page.

The spin Hamiltonian of $[Mn_{12}O_{12}(CH_3COO)_{16}\ (H_2O)_4]\cdot 2CH_3COOH\cdot 4H_2O$ is given by

$$\mathcal{H} = -DS_z^2 - BS_z^4 - g\mu_B H_z S_z + \mathcal{H}_T + \mathcal{H}_A + \mathcal{H}', \tag{1}$$

The first two terms represent the uniaxial magnetic anisotropy of the molecule ($D > 0$ and $B > 0$). The parameters, D and B, have been determined by high frequency EPR and neutron scattering experiments.[7,12,13] This spin-Hamiltonian, in a semiclassical view, describes a double potential well, in which opposite projections of the spin onto the z-axis are separated by an anisotropy energy barrier $\sim DS^2 + BS^4$ ($\sim$60 K) (see Fig. 1). The third term is the Zeeman energy due to the longitudinal component of an external magnetic field, $H_z = H\cos\theta$, where H is given in units of tesla (i.e. we set $\mu_0 = 1$) and θ is the angle between the field and the easy axis of the molecule. A magnetic field applied along the z-axis shifts the double well potential and the energies of the projections of the magnetization. At certain values of the z-axis field (resonance fields) the levels m and m' with antiparallel projections onto the z-axis have nearly the same energy, $H_k \sim kD/g\mu_B = 0.44$ T ($k = m + m'$) (see Fig. 1). At these resonances, MQT is turned on by interactions that *break* the axial symmetry and mix the levels m and m'. These off-diagonal terms have different origins: (a) $\mathcal{H}_T$ is the Zeeman interaction associated with the transverse component of the external magnetic field; (b) transverse anisotropy terms are included in $\mathcal{H}_A$; and (c) $\mathcal{H}'$ characterizes magnetic fields due to inter-molecular dipolar interactions and nuclear

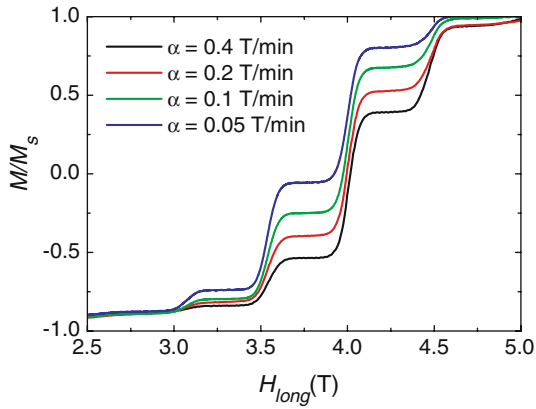

Fig. 2. (Color on-line) Magnetization versus field for a single crystal of Mn_{12}-ac for several sweep rates, $\alpha = dH/dt$. The measurements have been conducted in the pure quantum regime at $T = 0.6$ K.[11] The observed increases of the magnetization at regularly spaced field intervals, $H_k = D/g\mu_B \sim 0.44$ T, correspond to MQT at resonances $k = 6$, 7, 8, 9 and 10.

hyperfine. Off-diagonal terms in the Hamiltonian lift the degeneracy of the spin-levels at the resonances creating an energy difference between symmetric and antisymmetric superpositions of spin-projections that is known as the tunnel splitting, Δ (see Fig. 1).

Figure 2 shows magnetization curves measured at 0.6 K for several sweep rates of the longitudinal field, $\alpha = dH/dt$, for a single crystal of Mn_{12}-ac. The abrupt increases of the magnetization toward the equilibrium magnetization ($M/M_s = 1$) are due to MQT at the resonant fields. It is important to note for our discussion that MQT is observed at consecutive resonances. This has important implications for the understanding of MQT, because transverse anisotropy terms introduce selection rules and the only interaction that allows MQT at odd-resonances ($k = 1, 3, \ldots$) is a transverse magnetic field.

2.1. Transverse Interactions

The tunneling characteristics depend on the form of the off-diagonal terms. In this subsection, we will examine the consequences of the off-diagonal terms in the Hamiltonian on MQT. We consider both transverse magnetic field and anisotropy terms.

2.1.1. Magnetic Fields

The simplest expression for the off-diagonal part of the Hamiltonian of Eq. (1), involving a transverse magnetic field, H_T , is

$$\mathcal{H}_T = -g\mu_B H_T (S_x \cos\phi + S_y \sin\phi). \tag{2}$$

This represents the Zeeman energy for a field in the x–y plane at an angle ϕ with respect to the x-axis. The tunnel splitting, Δ, is very sensitive to this field, $H_T = \sqrt{H_x^2 + H_y^2}$. The dependence of Δ on H_T for small transverse magnetic fields ($H_T \ll H_D = 2DS/g\mu_B$, the anisotropy field) is given by Ref. 32,

$$\Delta_k(H_T) = g_k \left(\frac{H_T}{H_D}\right)^{\xi_k}, \tag{3}$$

where $g_k = \frac{2D}{[(2S-k-1)]^2} \times \sqrt{\frac{(2S-k)!(2S)}{k!}}$ and $\xi_k = 2S - k$. The power law dependence of Δ on H_T causes the tunnel splitting to vary by many orders of magnitude for transverse fields in the range of a few Tesla. This allows the study of MQT with a wide range of experimental techniques that go from quasi-static magnetization measurements ($\Delta/h \sim$ Hz) to high frequency

EPR experiments ($\Delta/h \sim 100\,\mathrm{GHz}$) simply by varying the magnitude of the applied transverse field.

2.1.2. *Transverse Anisotropies*

Now we examine the effect of transverse anisotropy terms in the Hamiltonian. Considering only the lowest order terms, $\mathcal{H}_A$ has the form

$$\mathcal{H}_A = E(S_x^2 - S_y^2) + C(S_+^4 + S_-^4). \tag{4}$$

The first term is the second order anisotropy which is allowed for SMMs with rhombic symmetry (e.g. Fe_8 (Ref. 33) and, as will be shown below, is also present in Mn_{12}-ac due to disorder that lowers the S_4 symmetry of the molecules.[16,18,19]) The second term is fourth order in the spin operators and is the lowest order anisotropy allowed with tetragonal symmetry. This form of the transverse anisotropy has been observed in EPR studies of several SMMs of tetragonal symmetry such as, Mn_{12}-ac[19], Mn_{12}-BrAc and Ni_4 (Ref. 34).

Let us consider in detail the consequences of each transverse anisotropy term. In Fig. 3, we show the shape of the classical anisotropy barrier separating antiparallel orientations of the spin z-projections (colored arrows). In the absence of transverse terms (Fig. 3a), the anisotropy barrier is determined by the uniaxial anisotropy of the molecules (first and second terms in Hamiltonian of Eq. (1)). These uniaxial anisotropy terms determine a hard

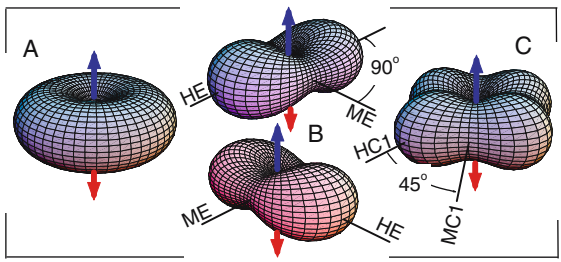

Fig. 3. (Color on-line) 3D representations of the anisotropy barrier. (a) Uniaxial anisotropy barrier in the absence of transverse anisotropy terms. The colored arrows represent the preferred orientation of the spin along the z-axis. (b) Anisotropy barriers corresponding to opposite signs of second order anisotropy, $\pm E(S_x^2 - S_y^2)$. The lines represent the hard (H) and medium (M) axes which are separated by 90 degrees. A change in the sign of E corresponds to a rotation of the transverse magnetic axes by 90 degrees. (c) Anisotropy barrier due to a fourth order anisotropy, $C(S_+^4 + S_-^4)$. In this case, there are two hard and two medium transverse axes separated by 45 degrees. A change of the sign of C produces a 45 degree rotation of the transverse magnetic axes.

anisotropy plane between opposite orientations of the spin states along the easy magnetic z-axis. Note that this barrier is isotropic in the $x-y$ plane. In this case, the tunnel splitting does not depend on the orientation of the transverse field in the hard plane.

This situation changes in the presence of a transverse anisotropy. Fig. 3b shows how the anisotropy barrier is modified by a second order anisotropy term of the form $E(S_x^2 - S_y^2)$. This term introduces one hard and one medium axis in the hard plane (the x–y plane) that are separated by 90 degrees. That is, for positive E the x is hard and y-axis is medium. A change of the sign of E leads to a 90 degree rotation of these axes. In this case, the tunnel splitting, Δ, depends on the azimuthal angle, ϕ, of the applied transverse field, H_T . A transverse magnetic field applied along the medium axis produces a larger tunnel splitting than the same field applied along the hard axis. This leads to an oscillatory dependence of Δ on ϕ with 2 maxima and minima separated by 90 degrees (see Fig. 4a). A second order anisotropy also introduces MQT selection rules. In the absence of a transverse field, this term only allows MQT for resonances that are even (i.e., $k = 2i$ with i an integer).

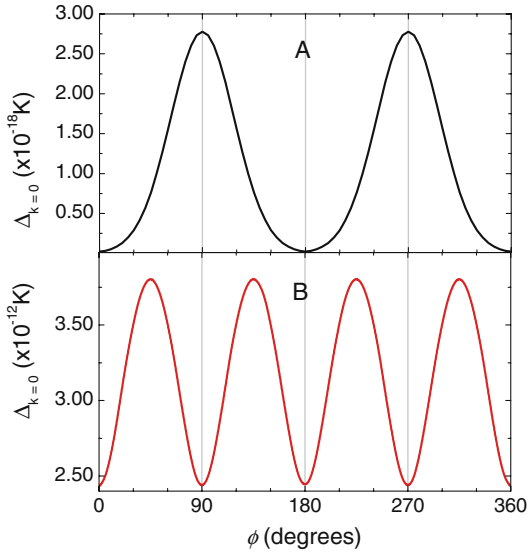

Fig. 4. Tunnel splitting of the ground state resonance, $k = 0$, as a function of the orientation (ϕ) of a transverse field of 0.3 T applied in the hard magnetic plane of a molecule for (a) only second, and (b) only fourth order anisotropy terms. We have used $D = 548$ mK, $B = 1.17$ mK, $E = 10$ mK and $C = 0.022$ mK in Eq. (1). The graphic clearly shows the 2-fold and 4-fold symmetries imposed by these different anisotropy terms.

Fig. 3c shows the modification of the anisotropy barrier in the presence of a fourth order anisotropy term of the form $C(S_+^4 + S_-^4)$. This anisotropy produces two medium and two hard axes in the hard plane. The separation between medium and hard axes is 45 degrees. Thus the tunnel splitting will have a 4-fold pattern of oscillations as a function of the angle of the transverse field, with maxima and minima spaced by a 45 degrees (see Fig. 4b). This term introduces a selection rule that allows tunneling transitions from the ground state for resonances that are a multiple of 4 ($k = 4i$). In Fig. 4 we show the expected behavior of the tunnel splitting of the ground state for resonance $k = 0$ versus the angle of the applied transverse field, $H_T = 0.3$ T. The tunnel splitting is calculated using the Hamiltonian of Eq. (1) with $D = 548$ and $B = 1.17$ mK and considering only second order anisotropy ($E = 10$ mK, Fig. 4a) and only fourth order anisotropy ($C = 0.022$ mK, Fig. 4b).

2.2. Disorder

Recent experimental results have shown that MQT in Mn_{12}-ac is modulated by off-diagonal terms that are generated by disorder. Disorder allows for anisotropy terms that are lower order in the spin-operators than those imposed by the average molecule site symmetry in SMM crystals. Disorder can also lead to tilts of the easy axes from the crystallographic easy axis.[9, 10, 17–19, 27, 28] The phenomena that have been explained by disorder can be summarized as follows: (a) observation of MQT relaxation at k-resonances that are not allowed by the quantum selection rules imposed by the symmetry of the molecule and (b) non-exponential magnetic relaxation which suggests the existence of a distribution of tunnel splittings.

Two distinct models of disorder have been proposed. Chudnovsky and Garanin[14,15] proposed that random line dislocations in a crystal lead, via magnetoelastic interactions, to a lower molecule symmetry and a broad distribution of tunneling rates. Subsequent magnetic relaxation experiments indeed showed the existence of a broad distribution of tunneling rates and were analyzed in terms of this model.[9,10] In contrast, Cornia *et al.*[16] suggested, based on detailed x-ray analysis, that variations in the position of the two hydrogen-bonded acetic acid molecules surrounding the Mn_{12}-ac clusters lead to a discrete set of molecules with lower symmetry than tetragonal. More recent magnetic relaxation experiments[18] and high frequency EPR experiments[19] have confirmed the latter model, showing a 2-fold symmetry of the tunnel splitting as a function of the direction of an external transverse field. Moreover, the observation of a distribution of transverse fields in Mn_{12}-BrAc[28] and tilts in Mn_{12}-ac[27] suggests that tilts of the easy axes of the molecules are responsible for the MQT relaxa-

tion at odd-k resonances; in the case of Mn_{12}-ac, these tilts are caused by the solvent disorder. We summarize these models and their consequences below.

2.2.1. Line Dislocations

Chudnovsky and Garanin[14,15] considered a random distribution of line dislocations with collinear axes to calculate a representative distribution of second order transverse anisotropies. They found: (a) the corresponding distribution of tunnel splittings is broad on a *logarithmic* scale; (b) the mode of the distribution is at $E = 0$; and (c), for small concentrations of dislocations, most molecules are far from the dislocation cores and the magnetic axes associated with the transverse anisotropy are oriented randomly. The first point can explain the non-exponential relaxation found in Landau–Zener relaxation experiments carried out at several MQT resonances, and at different longitudinal magnetic field sweep rates.[9] Furthermore, experiments in which a Mn_{12}-ac single crystal was treated with rapid thermal changes could be explained in terms of the dislocation model.[10] Point (b) leads to a distribution of tunnel splittings, with a very long tail towards small values of the tunnel splitting. In a more recent experimental study, a Landau–Zener method that involved crossing the same MQT resonance several times permitted the study of nearly the whole distribution of tunnel splittings in a Mn_{12}-ac single crystal at a single resonance.[17] The results obtained were compared to the distribution function proposed by Chudnovsky and Garanin. A distribution of second order anisotropies with mode at $E = 0$ was not able to explain the relaxation data. More recently, both magnetic relaxation and high frequency EPR experiments[18,19] confirmed the discrete nature of the distribution of transverse anisotropies and, moreover, the fact that the magnetic axes of the transverse anisotropy is also discretely distributed along particular directions in the hard anisotropy plane of the molecules, contrary to the random distribution expected from the dislocation model.

2.2.2. Solvent Disorder

From x-ray diffraction studies Cornia *et al.*[16] showed that the fourfold symmetry of Mn_{12}-ac molecules is lowered by disorder of the acetic acid molecules (two molecules with four possible sites). This gives rise to a set of six different molecules (4 of them with $E \neq 0$), with 7/8 or 88% of molecules thus having a non-zero second order transverse anisotropy. The fact that the second order anisotropy is generated by disorder in the solvent molecules implies that both the abundance and magnitude of the

E for each isomer could depend on the synthesis process as well as on the solvent losses that a particular crystal experienced prior to measurement. From x-ray data, Cornia *et al.* calculated the E parameters for the different isomers.[16] These should be taken as estimates, since the data were obtained from one crystal and the E-parameters were computed using an empirical model. Nonetheless, this model represents an important step in the understanding of MQT in Mn_{12}-ac.

The relevant points of the solvent disorder model can be summarized as follows: (a) there is a discrete set of E values in a sample. This means that the distribution of tunnel splittings is a discrete function with peaks at several $E \neq 0$ values. (b) There are equal populations of isomers having opposite signs of the second order anisotropy $\pm E$. This means that the medium and hard axes associated with each E value will be discretely distributed over the hard plane of the crystal with a separation of 90 degrees. And (c) the hard axes of the second order anisotropy are rotated away from the hard/medium axes corresponding to the fourth order anisotropy; this rotation angle depends on the precise details of the solvent structure, and is $\sim$30 degrees for Mn_{12}-ac. The first point has been confirmed by high frequency EPR experiments by the observation of discrete peaks in the absorption spectra that correspond to different discrete E values and have the angular dependence expected from this model.[19] The second point has been confirmed through magnetic relaxation measurements in which a portion of molecules having different signs of E have been studied.[17] The third point has been observed in EPR experiments and has implications for the MQT discussed below. We note that both models suggest the presence of tilts of the easy magnetic axes of the molecules. These latter results, which have recently been confirmed via density functional calculations.[35] will be presented in detail in the experimental sections of this paper.

2.3. The Effect of Disorder on MQT

In this section we will present model calculations of the dependence of the tunnel splitting on the angle and the magnitude of an external transverse field taking into account the presence of both second and fourth order anisotropies. These terms must be considered on an equal footing because they produce comparable tunnel splittings. This is seen as follows. In perturbation theory, the splitting between levels m and m' associated with the second order anisotropy is approximately $\Delta_E \sim D(E/2D)^{(m'-m)/2}$, while that associated with the fourth order anisotropy is $\Delta_C \sim D(C/2D)^{(m'-m)/4}$. Thus, provided $E^2 \sim DC$ these are comparable

in magnitude, *independent* of m and m'. This is the case for Mn_{12}-ac, as $E \sim 10^{-2}$ K and $C \sim 10^{-5}$ K and $D \sim 1$ K. For this reason there is an intricate interplay between these anisotropy terms that also occurs over a broad range of transverse magnetic fields, and can thus be probed both in EPR and MQT studies.

In Mn_{12}-ac these 2nd and 4th order transverse anisotropy terms have a different origin. The fourth order transverse anisotropy term is imposed by the symmetry of the molecule, while the second order term is generated by a distribution of solvent micro-environments. However, there is no reason to assume that these anisotropies are commensurate since they come from different sources; one is associated with the ideal S_4 symmetry, the other is disorder induced and lowers this symmetry. Therefore, we will consider a misalignment angle, β, between the magnetic axes associated with each transverse anisotropy term.

We write the transverse anisotropy part, $\mathcal{H}_{\mathcal{A}}$, of the Hamiltonian (Eq. (4)) as follows:

$$E(e_1(S_x^2 - S_y^2) + e_2(S_x \cdot S_y + S_y \cdot S_x)) + C(S_+^4 + S_-^4), \tag{5}$$

where,

$$e_1 = (\cos^2\beta - \sin^2\beta) \quad e_2 = 2\cos\beta\sin\beta. \tag{6}$$

This introduces an angle β between hard axes of the second and fourth order anisotropy terms (see Fig. 5), the 'E' and 'C' terms respectively.

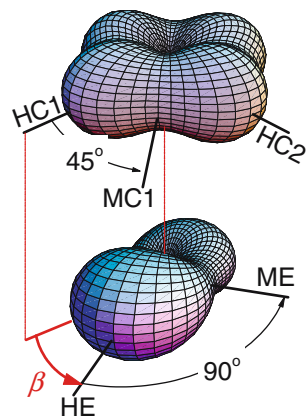

Fig. 5. (Color on-line) 3-D representation of the anisotropy barriers corresponding to fourth (upper graph) and second order (lower graph) anisotropies with an angle β between the corresponding hard axes.

In the next subsections we will show the effect of having a misalignment (β) on the symmetry of MQT and on the transverse field dependence of the tunnel splitting for different orientations of the applied field. The calculations have been done for parameters and conditions close to those shown in the experimental sections of this article. In the following, we consider in some detail the consequences of the solvent disorder model as this can adequately explain many of our experimental observations.

As mentioned, one of the important consequences of the solvent disorder model is the fact that there must be equal populations of molecules having opposite signs of E. This is because, on average, Mn_{12}-ac crystals have S_4 or tetragonal site symmetry. Note that Fig. 5 represents the picture for the molecules having $E > 0$. Thus there will be molecules in the sample with the magnetic axes of E rotated by 90 degrees with respect to those represented in Fig. 5.

2.3.1. Commensurate Transverse Interactions

We consider the case of $E > 0$ and $\beta = 0$ in the presence of large transverse field, as this field corresponds to that used in high frequency EPR experiments (Sec. 4). Figure 6 shows the behavior of the ground state tunnel splitting, $\Delta_{10,-10}$ (resonance $k = 0$), versus the angle, ϕ, of an external transverse field of 9 Tesla. The calculations have been done for $\beta = 0$, $D = 548$ mK, $B = 1.17$ mK, $C = 0.022$ mK and different values of E.

One interesting result in this figure is the observation of a fourfold pattern of maxima imposed by the fourth order anisotropy. There are four maxima in Δ that occur very close to the medium axes of C for

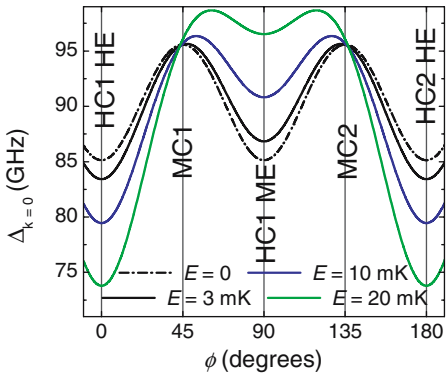

Fig. 6. (Color on-line) Behavior of the ground state splitting, $\Delta_{k=0}$, versus the orientation of a transverse field, $H_T = 9$ T, for $\beta = 0$ and different values of E > 0.

small values of E. Only when E becomes very large do the maxima move towards the medium axis of E to give, at high enough E-values ($E \gg 20\,\mathrm{mK}$), a twofold pattern of maxima. However, for the parameters estimated with the solvent disorder model, $E < 10 - 15\,\mathrm{mK}$, the tunnel splitting is expected to show fourfold maxima in the direction of the medium axes of C.

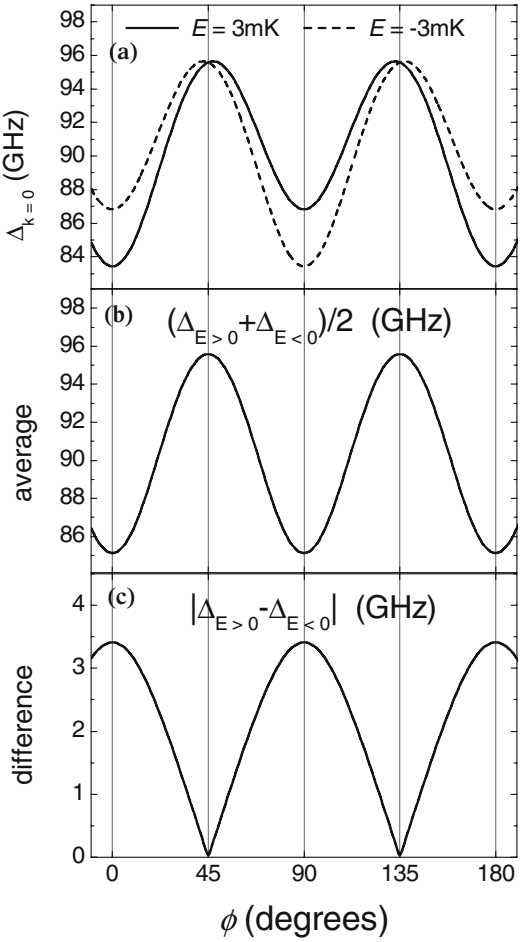

Fig. 7. (a) Ground state tunnel splitting, $\Delta_{k=0}$, versus the orientation of a transverse field, $H_T = 9\,\mathrm{T}$, for $\beta = 0$ and $E = +3\,\mathrm{mK}$ (solid line) and $E = -3\,\mathrm{mK}$ (dashed line). (b) Average value of the tunnel splitting assuming both E-signs. (c) Difference between the tunnel splitting values of $E > 0$ and $E < 0$.

Figure 7a shows the behavior of the ground state tunnel splitting, $\Delta_{k=0}$, for the same conditions as Fig. 6, that is for $\beta = 0$, but taking into account the equal population of molecules having opposite signs of E. In this case we have used $E = E_{\text{av}} = \pm 3\,\text{mK}$. The modulation of the fourfold symmetry by E is opposite for different signs of E. However, the maxima are approximately at the same position, independent of the sign of E. In Fig. 7b, we show the ϕ dependence of the average value of the tunnel splitting $(\Delta_{E>0} + \Delta_{E<0})/2$. This average exhibits a symmetric fourfold rotation pattern, the same as would be generated via only a fourth-order anisotropy. Therefore, a measurement of the average tunnel splitting of a crystal cannot distinguish between second and fourth order transverse anisotropies if there are equal populations of molecules with opposite signs of E.

The absolute difference between the tunnel splittings, corresponding to opposite signs of E, is shown in Fig. 7c. In this case, $\beta = 0$, the difference is maximal along the hard axes of C and vanishes along the medium axes of C. Importantly, this provides a means of inferring the presence of a second-order anisotropy through an appropriate experiment (this will be shown below and in Sec. 4).

2.3.2. Incommensurate Transverse Interactions

We now consider the effect of a misalignment, $\beta \neq 0$. Figure 8a shows the behavior of the ground state tunnel splitting, $\Delta_{k=0}$, versus the angle of the applied transverse field, $H_{\text{T}} = 9\,\text{T}$ for $E = 3\,\text{mK}$ and different values of β, from $\beta = -45^\circ$ to $\beta = 45^\circ$ in increments of 15 degrees. Note that the black line, $\beta = 0$, is the result presented in Fig. 7a. A misalignment $\beta \neq 0$ generates an asymmetry between the maxima of the tunnel splitting. For example, for $\beta = -45^\circ$, the maximum at $\phi = 45^\circ$ is bigger than the maximum at $\phi = 135^\circ$. Note that the hard axis of E (HE) for this value of β is $\phi = -45^\circ + n180^\circ$ (with n an integer) while the medium axis (ME) is along $\phi = 45^\circ + n180^\circ$. In general, even though the ME axis is at $\phi = \beta + (2n+1)90^\circ$, *the maxima of the tunnel splitting are in the direction of the medium axes of C*. The second order anisotropy introduces an asymmetric modulation of the maxima and minima of the tunnel splittings that depends on the value and the sign of E and on the misalignment angle β.

Figure 8b shows that the average value of the tunnel splitting is independent of the angle of misalignment β and has four maxima. All the results collapse in the same curve. So again a direct measurement of the average value of Δ would not give information about the misalignment between these anisotropies.

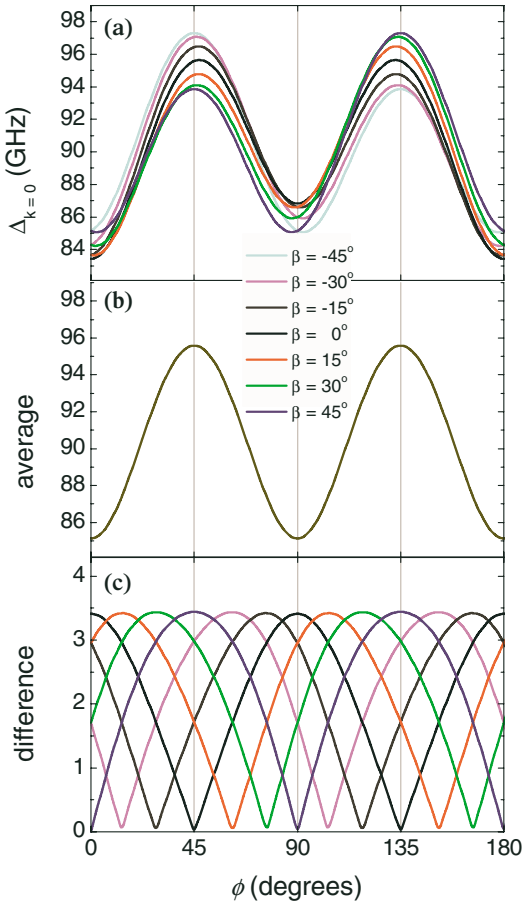

Fig. 8. (Color on-line)(a) Ground state tunnel splitting, $\Delta_{k=0}$, versus the orientation of a transverse field, $H_T = 9$ T, for $E = +3$ mK and different values of β. (b) Average value of the tunnel splitting assuming both E-signs for each value of β; all of the curves lie on top of each other. (c) Difference between the tunnel splitting values for $E > 0$ and $E < 0$ for different β-values.

Figure 8c shows the difference between $\Delta_{E>0}$ and $\Delta_{E<0}$ for the same parameters used in the previous calculation and different values of β from $-45°$ to $45°$. This difference has four maxima for all the angles β. However, the positions of the maxima are different for different β values. In fact, the position of the maxima depends directly on the value of β as $\phi_{max} = \beta + n90°$. Consequently, a measurement of this difference would not only provide the value of E but also give the angle of misalignment between second and fourth order transverse anisotropies.

We thus note that within the solvent disorder model the tunnel splitting of resonance $k = 0$ (the ground state degeneracy) at high transverse field values will show a fourfold rotation pattern with respect the angle of orientation of the applied field. This symmetry is modulated by the second order anisotropy. However, equal populations of molecules with opposite signs of E will give an average tunnel splitting with four maxima that is indistinguishable from that corresponding to the fourth order transverse anisotropy. The only way to determine the presence of second order anisotropy is by examining the difference of the tunnel splittings corresponding to molecules with opposite signs of E. The latter would give the value of E and the misalignment angle between the second and fourth order anisotropies. We will show how such measurements are possible via two different techniques in the experimental part of this paper.

2.3.3. Incommensurate Transverse Interactions and MQT

Let us now consider the situation relevant to understanding the physics of MQT in magnetic studies in which much smaller tunnel splittings are probed ($\sim 10^{-6}$ K). We will analyze the behavior of the splitting for resonance $k = 6$ ($m = -10$, $m' = 4$) versus the angle, ϕ, of a small external transverse field. The calculation has been done with the same D, B and C parameters of the Hamiltonian as those of the previous calculations. We have used $|E| = E_{av} = 3$ mK and a transverse magnetic field, $H_T = 0.35$ T, which corresponds to the situation studied in the dc Landau-Zener relaxation experiments that will be presented in Sec. 3.

The results are shown in Fig. 9. This situation is substantially different from that of the previous case of resonance $k = 0$. The tunnel splitting has a pattern that goes from two-fold maxima for $\beta = \pm 45^\circ$ to four-fold maxima for $\beta = 0$. Interestingly, *the maxima are in the directions of the medium axes of C independent of the direction of the medium axis of E*. For example, for $\beta = -30^\circ$ the two maxima of the tunnel splitting are at $\phi_{max} = 45^\circ, 135^\circ$ while the directions of the medium axis of E are $\phi_{ME} = \beta + 90^\circ = 60^\circ, 240^\circ$. So, for some β-values, the tunnel splitting exhibits a twofold pattern of maxima with position determined by the fourth order anisotropy. We have done these calculations for bigger values of E (not shown in this paper) that indicate that the range of β-values around $\beta = 0$ that exhibits fourfold symmetry is narrower the bigger the value of E. However, for E-values smaller than 30 mK the maxima positions are still determined by the fourth order anisotropy. This constitutes an unexpected result in a system with second and fourth order anisotropies that is first pointed out in this work and has important consequences for the interpretation of the experimental measurements that have been previously

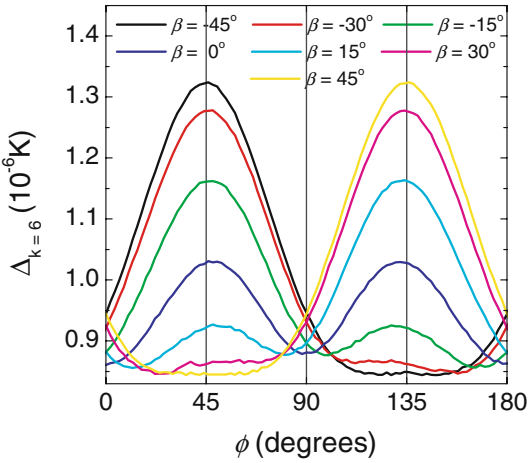

Fig. 9. (Color on-line) Ground state tunnel splitting, $\Delta_{k=6}$, versus the orientation of a transverse field, $H_T = 0.35\,T$, for $E = +3\,mK$ and different values of β.

published by some of the authors of this work,[18,19] as will be explained in the experimental Secs. 3 and 4.

We have calculated the average value of the tunnel splitting for different angles β assuming an equal population of molecules with different signs of E. The results are shown in Fig. 10. For all values of β there

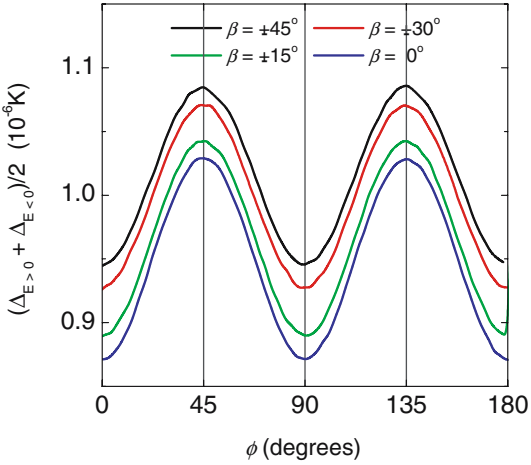

Fig. 10. (Color on-line) Average value of the ground state tunnel splitting, $\Delta_{k=6}$, for opposite signs of E ($|E| = 3\,mK$), versus the orientation of a transverse field, $H_T = 0.35\,T$, and for different values of β.

is clearly a fourfold rotation pattern of maxima of the average tunnel splitting with symmetric maxima and minima along directions determined by the fourth order anisotropy. Again, the only method to determine the E value and the relative orientation between C and E, β, is to study a subset of molecules having only one sign of E. In the latter case, depending on the value of β, there is a possibility that the molecules selected will also show fourfold symmetry (e.g. if $\beta \sim 0$). It would then not be possible to conclude that such molecules have a second order anisotropy. As we will show in Secs. 3 and 4 this is not the case experimentally. We will show that a selection of a subset of molecules with one sign of E shows twofold symmetry which indicates that the angle β of misalignment is close to $\beta \sim \pm 45^\circ$ (specifically, $\beta = -30^\circ$).

2.3.4. Disorder and Berry Phase Effects

Quantum phase interference is one of the most important phenomena observed in SMMs. Interference effects (Berry phase) in MQT were first discussed by Loss[36] and calculated for a nanomagnet with a biaxial anisotropy by Garg.[37] This phenomenon is due to interference of the quantum tunneling trajectories of the magnetization and has been clearly observed in two SMMs to date.[33,38] The first observation of the Berry phase was by Wernsdorfer and Sessoli[33] in the Fe_8 SMM. Fe_8 has both second and fourth order transverse anisotropy. The observation of quantum oscillations was done by applying a transverse field along the direction of the hard axis of the second order anisotropy (HE), which in this case also corresponds to the direction of one of the hard axes of the fourth order anisotropy term, $\beta = 0$. Figure 11 shows the dependence of the tunnel splitting of resonance $k = 0$ on the external field applied along $\phi = 0$ (hard E anisotropy axis) and $\phi = 90^\circ$ (medium E anisotropy axis). We have used the parameters given in Ref. 33.

The field spacing between quantum tunneling oscillations of Fig. 11 can be described in terms of the anisotropy parameters D and E of the Hamiltonian using a semiclassical approach,[37]

$$\Delta H = \frac{2k_B}{g\mu_B}\sqrt{2E(E+D)}. \tag{7}$$

This is $\sim 0.23\,\mathrm{T}$ for Fe_8 which is smaller than the spacing resulting from the exact diagonalization of the Hamiltonian including fourth order transverse anisotropy, $\Delta H = 0.41\,\mathrm{T}$, and was observed in reference.[33] The reason is that Eq. (7) only considers the presence of a second order anisotropy.[39] Note that the authors of Ref. 33 assumed commensurate anisotropies to fit the data, thus the angle between the HE and HC1 axes is

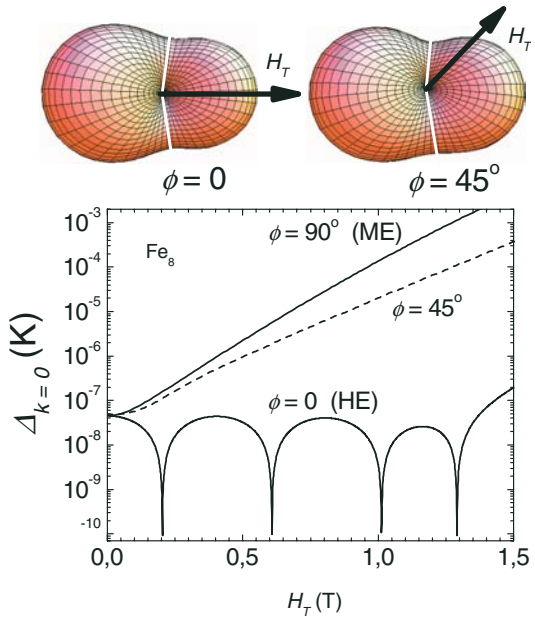

Fig. 11. (Color on-line) Fe_8 ground state tunnel splitting, $\Delta_{k=0}$, versus the magnitude of a transverse field applied along the hard (HE) and the medium (ME) anisotropy axes. The parameters used in this calculation were taken from Ref. 33. The drawings above represent the $x - y$ plane projections of the anisotropy barrier for Fe_8 in the presence of a transverse field applied at different angles ϕ. The white lines show two hypothetical quantum tunneling trajectories. When H_T is applied along the hard anisotropy axis, $\phi = 0$, the barrier remains symmetric with respect to the field. In this case, the trajectories interfere. For transverse fields not aligned with the hard axis, an asymmetric distortion of the barrier leads to non-equivalent MQT trajectories, destroying the interference.

$\beta = 0$ (see Fig. 5). We also have used collinear second and fourth order anisotropy terms in the calculated data shown in Fig. 11. So we can see that the effect of having a fourth order anisotropy that is commensurate with a second order anisotropy, $\beta = 0$, only modifies the pattern of oscillations but not their structure and shape. Quantum tunneling oscillations were also observed in $[Mn_{12}]^{-2}$ which has a dominant second order transverse anisotropy.[38] In this case, the spacing between oscillations was given by Eq. 7.

Park and Garg[40] calculated the quantum tunneling oscillations in a system with only fourth order transverse anisotropy using the Hamiltonian of Mn_{12}-ac (Eq. (1)). Figure 12 shows calculations of the tunnel splitting for different resonances by using Eq. (1) with $D = 556\,\text{mK}$, $B = 1.1\,\text{mK}$ and $C = 0.03\,\text{mK}$.

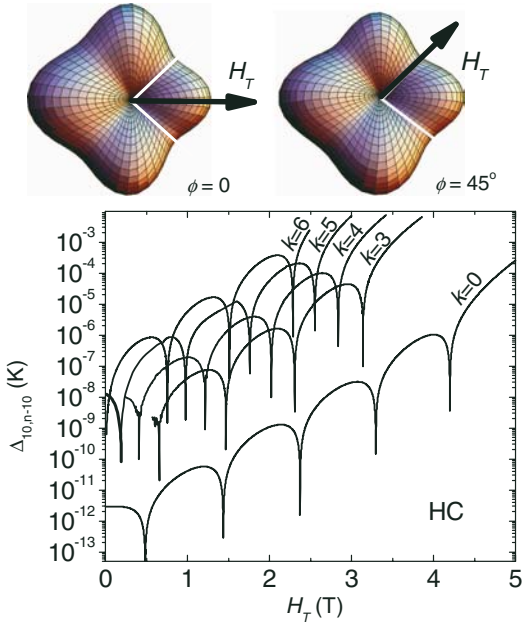

Fig. 12. (Color on-line) Transverse field dependence of the tunnel splittings for Mn_{12}-ac, for several resonances, assuming only fourth order anisotropy. The transverse field is applied along one of the hard axes of C (HC). The drawings above the figure show the distortion of the anisotropy barrier due to a transverse field applied at different angles with respect to the hard axes of the fourth order anisotropy. White lines represent different tunneling trajectories.

In order to take into account the effect of a misalignment, $\beta \neq 0$, between second and fourth order anisotropies we have calculated the dependence of the ground state tunnel splitting on the magnitude of an external transverse field applied along different characteristic directions in the hard plane of a molecule. For this, we have used $\beta = -30^\circ$, $D = 548\,\text{mK}$, $B = 1.17\,\text{mK}$ and $C = 0.022\,\text{mK}$ and different values of $E > 0$. For clarity, this situation corresponds to having the following directions for the characteristic transverse anisotropy axes: $\phi_{\text{HC}} = 0, 90^\circ, 180^\circ, 270^\circ$, $\phi_{\text{MC}} = 45^\circ, 135^\circ, 215^\circ, 305^\circ$, $\phi_{\text{HE}} = \beta + n180^\circ = -30^\circ, 150^\circ$ and $\phi_{\text{ME}} = 60^\circ, 240^\circ$.

Examining the result for $\beta = -30^\circ$ in Fig. 9 (red curve) one can see that the tunnel splitting has twofold symmetry with maxima at $\phi = 45^\circ, 225^\circ$ and minima at $\phi = 135^\circ, 315^\circ$. These directions correspond to the medium axes of C (MC1 and MC2). We have thus calculated the dependence of the ground state tunnel splitting for resonances $k = 5, 6$ and 7 for the field applied along MC1 and MC2. These are shown in Fig. 13a, b

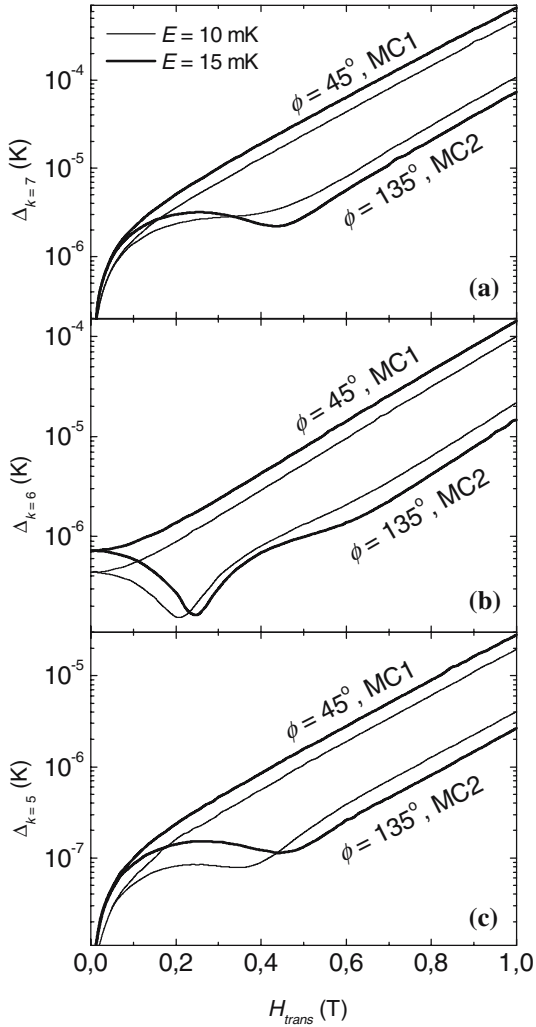

Fig. 13. Transverse field dependence of the ground state tunnel splitting of resonances $k=5$, $k=6$ and $k=7$ for Mn_{12}-ac, with $E=10\,\mathrm{mK}$ and $E=15\,\mathrm{mK}$. The transverse field is applied along the $\phi=45^\circ$ and $\phi=135^\circ$ directions, which correspond to the positions of the maxima and minima of Δ for a misalignment angle $\beta=-30^\circ$.

and c respectively, for a transverse field applied along $\phi=45^\circ$ (tunnel splitting maximum, MC1 axis) and $\phi=135^\circ$ (tunnel splitting minimum, MC2 axis) using $E=10\,\mathrm{mK}$ (thin lines) and $E=15\,\mathrm{mK}$ (thick lines). Figure 13 shows how the minimum in the tunnel splitting moves to higher fields and becomes deeper as E increases.

The results show a very different structure and shape of the Berry phase oscillations as compared to the case when both anisotropies are commensurate. Note that the orientations we used for the applied transverse field correspond to the medium axes of the fourth order anisotropy where one does not expect to have Berry phase oscillations. Moreover, these two orientations, $\phi = 45^\circ$ and $\phi = 135^\circ$, do not coincide with the hard axis of the second order anisotropy, which for $\beta = -30^\circ$ is along $\phi = -30^\circ + n180^\circ$.

In order to have a more complete picture of the effect of second and fourth anisotropies with incommensurate axes on the Berry phase phenomena we have calculated the dependence of the ground state tunnel splitting of resonance $k = 7$ on the magnitude of a transverse field applied at different angles, from $\phi = 45^\circ$ (which correspond to one of the medium axes of C) to $\phi = 225^\circ$ (which correspond to the opposite orientation of the field along the same hard C-axis). The results are shown in a color contour plot in Fig. 14. The first thing to point out is that the tunnel splitting still has zeros in this situation. However, the most significant fact is that these zeros do not appear at an angle characteristic of the transverse anisotropies. Moreover, the structure, shape and position of the zeros are completely independent of the Berry phase correspond-

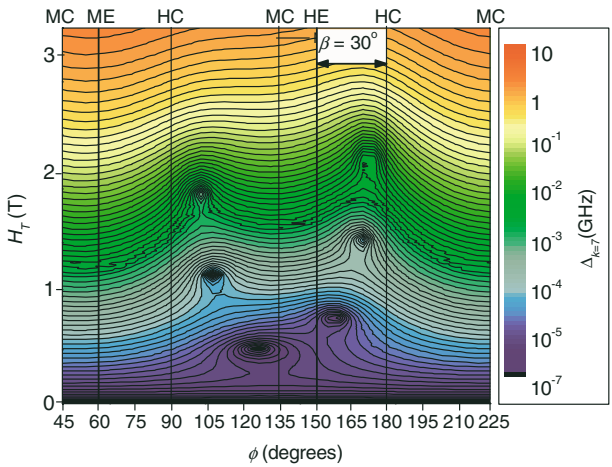

Fig. 14. (Color on-line) Color contour plot of the transverse field dependence of the ground state tunnel splitting of resonance $k = 7$ for different angles ϕ for a misalignment, $\beta = -30^\circ$, between the hard anisotropy axes of E and C. The vertical lines represent the orientations of hard and medium axes of the second and fourth order anisotropy terms. This misalignment generates a new and interesting pattern of Berry phase zeros that does not correspond to any of the anisotropies separately.

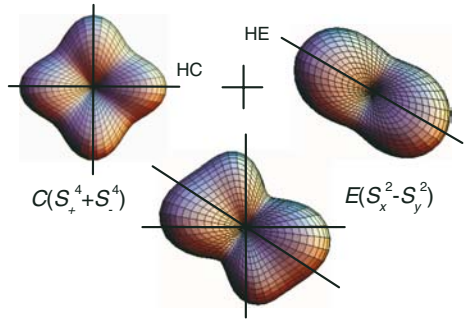

Fig. 15. (Color on-line) Projection of the anisotropy barrier onto the $x-y$ plane for second (right-upper graphic) and fourth (left-upper graphic) order transverse anisotropy terms. The addition of both anisotropies leads to an asymmetric barrier (lower graphic) that makes it difficult to see the orientations of a transverse field that would generate equivalent quantum tunneling trajectories and, therefore, Berry phase interference phenomena.

ing to each anisotropy term separately. Note that the calculations shown in Fig. 13 correspond to transverse fields applied along $\phi = 45^\circ$ and 135° which correspond to the directions of the maximum and minimum values of the tunnel splitting of Fig. 9, respectively. In the case of $\phi = 135^\circ$ the tunnel splitting is close to one of the zeros ($\phi \sim 125^\circ$ and $H_T \sim 0.4$ T in Fig. 14) but far from all the others, explaining the observation of only one incomplete oscillation in Fig. 13a. This new and unusual structure of the Berry phase zeros can be better understood by looking at the graphic representation of the anisotropy barrier of Fig. 15. The addition of second (right-upper illustration in Fig. 15) and fourth order (left-upper) transverse anisotropies in a SMM leads to an asymmetric barrier (center-lower) where symmetry does not permit a direct identification of the field that generates equivalent quantum tunneling trajectories that can interfere.

From the results, we can conclude that the combination of incommensurate transverse anisotropy terms of different order in the spin-operators can lead to an interesting situation in which the resulting magnetic response does not depend in any simply way on the form of either anisotropy term separately. The parameters used in the above simulation were chosen because they are within the range of values that can explain the experimental results presented in Secs. 3 and 4.

3. MAGNETIC RELAXATION EXPERIMENTS

We have carried out magnetic relaxation measurements in a single crystal of deuterated Mn_{12}-ac in the pure quantum regime ($T = 0.6$ K)

in which relaxation is by MQT without thermal activation over the anisotropy barrier.[11] Deuterated crystals were studied because the purity of the chemicals used in the synthesis leads to very high quality crystals.[41]

We have used a high sensitivity micro-Hall effect magnetometer[42] to measure the magnetic response of a Mn_{12}-ac single crystal of $\sim$100 micrometer size and needle shape. We measure the longitudinal component of the magnetization of the sample (z-component) by placing the crystal with one of its faces parallel to the sensor plane and one end just over the cross point of the micro-Hall sensor. The magnetometer was placed inside a low temperature He^3 system. A superconducting vector-field magnet was used to apply high magnetic fields at arbitrary directions with respect to the crystal axis.

3.1. Landau–Zener Method

The Landau–Zener (LZ) method has been used to study quantum tunnel splittings in SMMs[33] and has become a powerful tool to check for distributions of dipolar and nuclear interactions,[38] molecular micro-environments[9,10,17,18] or internal transverse magnetic fields[28] in these materials. The method consists in crossing a MQT resonance by sweeping the longitudinal magnetic field at a constant rate, $\alpha = dH/dt$, and measuring the fractional change of the magnetization in the process. The anti-crossing of the spin levels m and m' of resonance $k = m + m'$ is shown in the inset of Fig. 16. For an ideal system of non-interacting and monodisperse SMMs, and for low enough temperatures (where thermal relaxation is negligible), the normalized change of magnetization, $(M_{\text{before}} - M_{\text{after}})/(M_{\text{before}} - M_{eq})$, is related to the probability for a molecule to reverse its magnetization by quantum tunneling. The bigger the MQT probability the larger the magnetization change will be. This MQT probability is related to the tunnel splitting, Δ, by the LZ formula,[43]

$$P_{\text{LZ}} = 1 - \exp\left(-\frac{\pi\Delta^2}{2\nu_0}\frac{1}{\alpha}\right), \tag{8}$$

where $\nu_0 = g\mu_{\text{B}}(2S-k)$ and $\nu_0\alpha$ is the energy sweep rate. $R_{\text{LZ}} = 1 - P_{LZ}$ is the probability for a molecule to remain in the metastable state $|m'\rangle$ after crossing the resonance.

It is important to note that this relation is only valid if the internal energy sweep rate a single molecule experiences is proportional to the external sweep rate of the magnetic field. This is not satisfied if there are internal dipolar or nuclear fields. In fact, it has been shown in Fe_8[38]

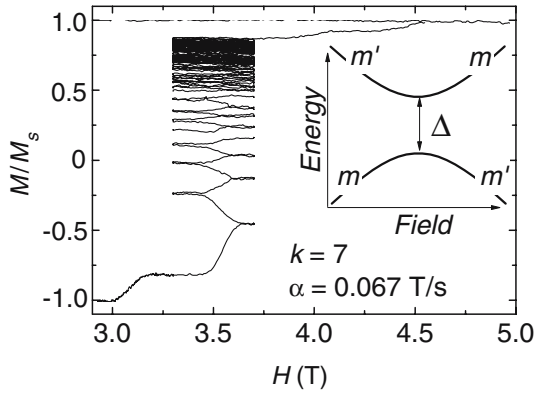

Fig. 16. Landau–Zener multi-crossing experiment in a Mn_{12}-ac single crystal measured at 0.6 K by sweeping the longitudinal magnetic field at a constant rate, $\alpha = 6.6 \times 10^{-3}$ T/s, multiple times across the $k = 7$ resonance. The inset shows a representation of the energy levels, m and m', at the anti-crossing point.

and Mn_{12}-ac[17] that changing dipolar fields lead to deviations from the LZ formula. In order to avoid these effects the external sweep rate must be fast enough to have small magnetization change (i.e. small changes of dipolar fields) in the crossing process. The critical lower value of the magnetic field sweep rate, α_c, that is needed to avoid this situation has been determined to be 10^{-3} T/s for Mn_{12}-ac.[17] Due to this, all the experiments presented in this section have been conducted with $\alpha > \alpha_c$.

3.2. Multi-Crossing Landau–Zener Measurements

When there is a distribution of quantum splittings in the sample each molecule has a different MQT probability and the relaxation of the magnetization should reflect this fact. In this case, the MQT probability depends on the distribution of tunnel splittings of the molecules that are in the metastable well before crossing a resonance. After a crossing of a resonance, those molecules with the largest tunnel splitting values and, consequently, the highest MQT probability will represent the maximum contribution to the fractional change of the magnetization. Correspondingly, those molecules with smaller tunnel splitting values will remain in the metastable well. Due to this, the LZ relaxation method can be used to determine the distribution of tunnel splittings in a sample, and to select different parts of the distribution for independent study, as we will show in subsection 3.3.

In order to extract the complete distribution of tunnel splittings in Mn_{12}-ac we have used a modification of the LZ method that consists of crossing a resonance multiple times, both for increasing and decreasing fields. As we have stated previously, molecules in the metastable well having the largest tunnel splitting values are most likely to relax in any given crossing of a resonance. Once a molecule has relaxed, it will no longer exhibit dynamics in subsequent crossings of the same resonance. Thus, only those molecules with the largest probability of tunneling, and which did not already tunnel, can contribute to the relaxation during subsequent crossings of the resonance. The repetition of this procedure many times enables a determination of the distribution of tunnel splittings in the sample over several orders of magnitude. We show an example of this multi-crossing LZ procedure for resonance $k = 7$ in Fig. 16.

In a multi-crossing LZ measurement the probability to remain in the metastable well after crossing a resonance n-times is given by,

$$R_{\mathrm{LZ}n} = \exp\left(-\frac{\pi\Delta^2}{2\nu_0}\frac{1}{\alpha_{\mathrm{eff}}}\right), \tag{9}$$

where $\alpha_{\mathrm{eff}} = \alpha/n$. If this expression describes the physics, then relaxation curves recorded at different sweep rates should scale when plotted as a function of the effective sweep rate. This can be clearly observed in Fig. 17, where we show LZ multi-crossing relaxation measurements of resonances $k = 6, 7$ and 8, carried out at different sweep rates $\alpha > \alpha_c$ (3.33×10^{-3} to 1.33×10^{-2} T/s). Small differences in the results were observed in three different crystals that were synthesized in the same way. These results clearly show that the MQT relaxation rate is not exponential and indicate the presence of a distribution of tunnel splittings within the sample. These results confirm previous experimental observations of non exponential relaxation in Mn_{12}-ac.[6,8–10] Moreover, the large fraction of the relaxation that we are able to observe with this method gives direct information on the width of the distribution of tunnel splittings.

We have assumed a log-normal distribution of tunnel splittings to explain our observations. We take the form,

$$f(x) = Aexp\left(-\frac{(x-x_c)^2}{\sigma^2}\right), \tag{10}$$

where $x = \log\Delta$ and $x_c = \log\Delta_c$, Δ_c and σ represent the center and the width of the distribution, respectively. The fits of the relaxation curves that are shown in Fig. 17 (solid lines) have been obtained by using,

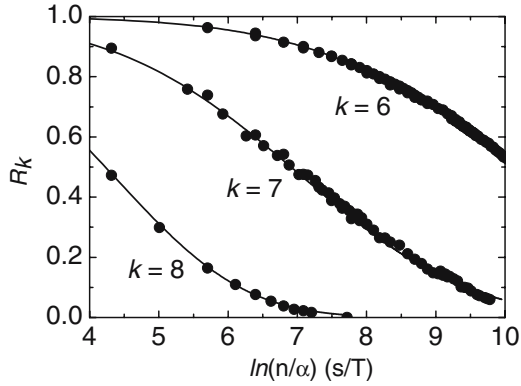

Fig. 17. Landau–Zener probability to remain in the metastable well in multi-crossing relaxations of resonances $k = 6$, 7 and 8 using different sweep rates (3.33×10^{-3} to 1.33×10^{-2} T/s). All the measurements were performed beginning with a saturation magnetization at $T = 0.6$ K.

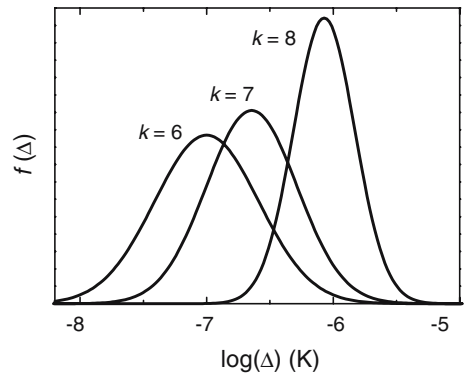

Fig. 18. Log-normal distribution functions extracted from the fit to the LZ relaxation curves of Fig. 17.

$$R(\alpha, n) = \int_{-\infty}^{\infty} R_{lz}(\alpha, \Delta, n)\, f(\log \Delta) d \log \Delta, \tag{11}$$

with x_c and σ as free parameters. The resulting fits are in excellent accord with the experiments. The resultant distribution functions for resonances $k = 6, 7$ and 8 are shown in Fig. 18. The center of the distribution increases with the resonance number, k, while the width remains almost constant for different resonances, being somewhat narrower for resonance $k = 8$.

In Sec. 2.2 we have discussed the two models that have been proposed to explain the presence of a broad distribution of tunnel splittings in terms of disorder. Before analyzing our results, note that a second order transverse anisotropy allows transitions for resonances $2i$, while a fourth order anisotropy, which is imposed by the symmetry of the molecules, only allows MQT relaxation for resonance numbers which are a multiple of 4, $4i$. Thus, a comparison between relaxation curves recorded at resonances $k=6$ and 8 should give us information about the origin of the tunnel splittings in this material. The relation between the tunnel splitting and the second order anisotropy is given by the next formula which follows from perturbation theory:[32]

$$\ln(\Delta_k/g_k)/\xi_k = \ln\left(\frac{E}{2D}\right), \tag{12}$$

where g_k and ξ_k depend on k, S and D (see Ref. 32) and were given in Section 2.1. Through this expression we can infer the distribution of second order anisotropy parameters, $f(\ln(E/2D))$, by taking the log-normal distributions used to fit the relaxation curves of resonances $k=6$ and $k=8$. The results are shown in Fig. 19. The fact that both distributions do not scale when plotted as a function of $\ln(E/2D)$ indicates that second order anisotropy can not be the only origin of tunnel splittings within the sample.

The distribution function of the second order anisotropy parameter predicted by the line dislocations model is given by Ref. 15,

$$f_{\mathrm{L}}(x) \cong \frac{1}{2\sqrt{\pi}\,\tilde{E}_c}\exp\left(x - \frac{e^{2x}}{(2\tilde{E}_{\tilde{c}})^2}\right), \tag{13}$$

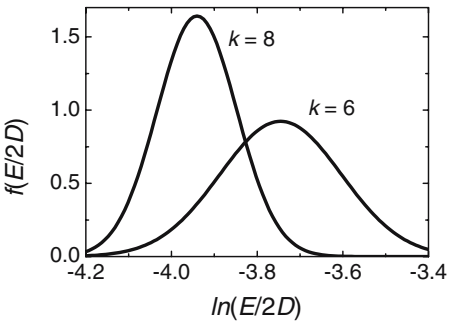

Fig. 19. Distribution of the second order anisotropy parameter inferred from the log-normal distribution functions of resonances $k=6$ and 8 of Fig. 18 using the expression of Eq. (11).

where $x \equiv \ln \tilde{E}$ with $\tilde{E} = E/2D$. $\tilde{E}_{\tilde{c}}$ is the width of the distribution of the anisotropy parameter $\tilde{E}$. $\tilde{E}_{\tilde{c}}$ depends on the geometry of the crystal and on the concentration of dislocations per unit cell, c. Note that the mean value and width of the distribution given by this expression are not independent variables. By using this distribution with Eq. (11) we have fit the relaxation curve recorded at resonance $k = 6$. The only free parameter in the fit is $\tilde{E}_{\tilde{c}}$. The result is shown in Fig. 20 (thin line) where the log-normal distribution extracted from our previous fit of the same relaxation curve has been included for comparison (thick line). We have chosen the mean value to be at the same position as that of the log-normal distribution. The value of $\tilde{E}_{\tilde{c}}$ used to fit the data corresponds to a concentration of dislocations per unit cell of $c \sim 10^{-4}$. Clearly, the width of this distribution is many orders of magnitude bigger than the log-normal distribution used to fit our data. This is due to the fact that the distribution of E predicted from the line dislocations model has a most probable value at $E = 0$, which explains the long tail observed for low tunnel splitting values. Consequently, line dislocations would produce a much broader relaxation curve than that observed in the experiments. Our data indicate that a distribution of second order anisotropy with a non zero mode is needed to explain the MQT relaxation in Mn_{12}-ac.

We want to note that we were able to fit the relaxation curves by using a discrete multi-peak distribution of E values similar to that expected from the solvent disorder model.[16] However, it was necessary to include a Gaussian width to each peak of the distribution in order to fit

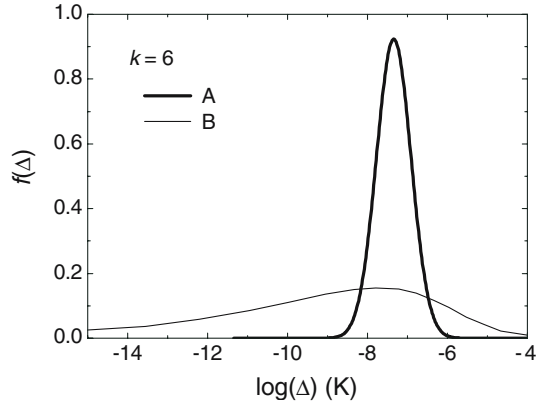

Fig. 20. Tunnel splitting distribution of resonance $k = 6$ expected from the line-dislocation model (thin line) compared with the log-normal distribution that fits the experimental data (thick line).

the data.[17] The values of the peak centers of this distribution for resonance $k = 6$ are $x_{c,1} = -7.19(-7.0525)$, $x_{c,2} = -8.55(-8.1749)$, and $x_{c,3} = -6.60(-6.7995)$, (the values in parenthesis are extracted from Ref. 16). The width of each peak is $W_i = x_{c,i}/50$ and the height of each peak was taken to be proportional to the population of the corresponding isomer given in Ref. 16.

To conclude this subsection, we have shown that a multi-crossing LZ method allows the determination of the complete distribution of tunnel splittings for several resonances in SMMs. Our results suggest that a distribution of second order transverse anisotropies with a non zero mode is necessary to explain the experimental data. The solvent disorder model provides such a source and a discrete multi-peak distribution of tunnel splittings can be used to fit our data. However, an additional source of disorder (e.g. line-dislocations or point defects) that introduces a small broadening of the these peaks is also necessary to model the experimental data.

3.3. MQT Symmetry Measurements

In this subsection, we will present LZ relaxation experiments carried out in the pure quantum regime ($T = 0.6\,\mathrm{K}$). In order to check the MQT symmetry imposed by the transverse terms of the Hamiltonian we have studied the LZ relaxation of the magnetization by sweeping an external longitudinal field, H_L, at a constant rate, α, across a resonance k in the presence of an external transverse field, H_T , applied at arbitrary directions, ϕ, with respect to the crystallographic axes of a Mn_{12}-ac single crystal. As we have shown in Section 2 (i.e. see Fig. 4), MQT has an oscillatory response as a function of the orientation of a transverse field. This leads to maxima and minima in the MQT relaxation rates whose positions and symmetry depend on the transverse anisotropy term that generates the tunnel splittings. To recall, a fourth order anisotropy term would generate a fourfold rotation pattern in the MQT probability with maxima spaced by 90 degrees, while a twofold rotation pattern with spacing between maxima of 180 degrees is expected from a second order anisotropy term in the Hamiltonian. When incommensurate transverse anisotropy terms of different order are present, the symmetry of the MQT relaxation rates depends on the relative orientation between the anisotropy axes, as discussed in Sec. 2.2.

A single crystal of Mn_{12}-ac was placed over a high sensitivity micro-Hall magnetometer as described in the first paragraph of this section. However, for these studies it is very important to know the exact orientation of the crystallographic axes with respect to the direction of the

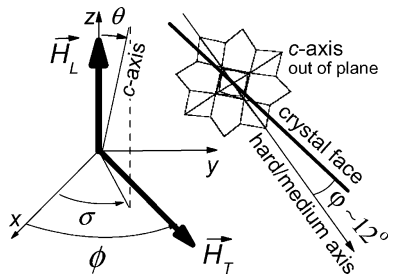

Fig. 21. Schematic representation of the orientation of the c-axis (easy axis) of a crystal with respect to the axes of the applied external magnetic field (x, y, z). The misalignment is determined by θ and σ. The misalignment between the transverse magnetic axes of the Mn_{12}-ac molecules, and one of the faces of the crystal ($\varphi \sim 12^\circ$), is also shown.

external magnetic field. Figure 21 shows a sketch of the orientation of the c-axis of the crystal with respect to the external magnetic field. Note that, in Mn_{12}-ac, the c-axis corresponds to the easy magnetic axis of the molecules. However, there is a misalignment of $\varphi \sim 12^\circ$ between the transverse magnetic axes (imposed by the fourth order anisotropy of the molecules) and the crystallographic axes. This is also shown in Fig. 21.

During the manual alignment of the crystal one of its faces was placed coplanar with the micro-Hall sensor plane with the help of a microscope. However, there exists an uncertainty of about ± 5 degrees in this orientation. This misalignment is represented by the angles θ and σ in Fig. 21 and can be determined experimentally through the magnetic measurements described below. The main implication of this misalignment is that there is a transverse field component due to the high longitudinal field applied along the z-axis that depends on the angles θ, σ and ϕ. The latter is the angle of application of the external transverse field with respect to the x-axis. Due to this, the total transverse field felt by the molecules in the presence of a constant transverse field, H_T, applied along ϕ and with a longitudinal field, $H_L = H_z \cos\theta \sim H_z (\cos\theta \sim 1$ for θ small) is given by,

$$H^2 \sim [H_T \cos(\phi - \sigma) - H_L \sin\theta]^2 + [H_T \sin(\phi - \sigma)]^2. \tag{14}$$

Thus, the transverse field felt by the molecules will have a minimum value for $\phi = \sigma$ and a maximum for $\phi = \sigma + 180^\circ$ with $H_L > 0$. The opposite situation would be found for $H_L < 0$. As we will show, once the misalignment angles are known, an algorithm can be used to correct the applied fields in order to have a constant transverse field during the measurements, independent of the angle of application of the external fields.

In our first experiment we have studied the MQT relaxation rates of several resonances in the presence of a constant transverse field applied at

arbitrary directions with respect to the crystallographic axes. The experiment was done as follows: We start with the initial magnetization of the sample equal to positive saturation, $M_{\text{initial}} = +M_s$, by applying a high longitudinal magnetic field, $H_L = 6\,\text{T}$. For this initial situation, all of the molecules of the crystal were in the $m = +10$ level in one of the energy wells. Then we turn on a transverse magnetic field, $H_T = 0.4\,\text{T}$, applied along a direction, ϕ, and sweep the longitudinal field at a constant rate, $\alpha = -6.6 \times 10^{-3} T/s$ to $H_L = -6T$. We measured the magnetization change in several resonances k and determined the MQT probability, $P_{LZ} = (M_{\text{before}} - M_{\text{after}})/(M_{\text{before}} - M_{\text{eq}})$, where, in this case, $M_{\text{eq}} = -M_s$. Note here that all the molecules within the crystal contribute to the relaxation. We repeated this procedure for different angles ϕ from 0 to 360 degrees.

The behavior of the measured MQT probability as a function of ϕ is shown in Fig. 22 for resonances $k = 5$ and $k = 6$. The results clearly show fourfold maxima in the tunneling probability spaced by 90 degrees ($\phi_{\max} = 60^\circ; 150^\circ; 240^\circ$ and 330°) for both resonances. Note that $k = 5$ and 6 are the first observed resonances and $\sim 35\%$ of the magnetization relaxes. This means that molecules that contribute to this relaxation are mainly those with the biggest tunnel splitting values within the distribution.

There is also a one-fold contribution that is represented by a continuous line in Fig. 22 with the result for resonance $k = 6$.[44] This oscillation is due to the misalignment of the c-axis of the crystal with respect to the applied magnetic field. This misalignment is represented by the angles θ and σ and can be determined through magnetic measurements. From the results shown in Fig. 22 we find $\sigma = 80^\circ$ (where we observe the maximum value of the one-fold contribution). To obtain θ, we measured the

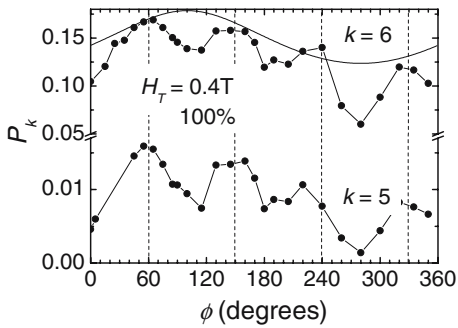

Fig. 22. Measured MQT relaxation probability for resonances $k = 6$ and $k = 7$, as a function of the orientation of the applied transverse field, $H_T = 0.4\,\text{T}$, relative to one of the faces of the crystal. The measurements where carried out starting from saturation (all the molecules within the crystal contributed to the relaxation).

behavior of the MQT probability of resonance $k=6$ for different magnitudes of the transverse field from -0.4 to 0.4 T applied along $\phi=\sigma$. The transverse field value for which the probability is minimum (null real transverse field) gives the angle of misalignment θ through $H_T(P_{min}) = H_L \sin\theta$, where $H_L \sin\theta$ is the transverse projection of the longitudinal field. The value extracted for the misalignment is $\theta = 0.3^\circ$. The effect of this misalignment on the transverse field is larger the greater the resonance number. We do not show the results for higher resonances, such as $k=8$, because the fourfold symmetry is almost unobservable due to the high one-fold contribution of the misalignment.

In order to measure the response of the MQT probability versus the angle ϕ in other parts of the tunnel splitting distribution we have conducted LZ relaxation experiments in the following manner. We select a small fraction of molecules with the smallest tunnel splittings of the distribution, in contrast to the biggest values that were analyzed in the previous experiments. The measurement method is presented in Fig. 23. We start with $M=-M_s$ by applying a high negative longitudinal magnetic field, $H_L=-5$ T. Then we sweep the longitudinal field at a constant rate, $\alpha = 6.6\times10^{-3}$ T/s, up to $H_L=+4.2$ T (just after crossing resonance $k=8$) and sweep it back to zero, crossing again resonances $k=8,7,6,\ldots$ The whole selection process is done in the absence of a transverse field. After that, the final magnetization of the sample is $M=0.4M_s$. This means that 70% of the molecules have relaxed to the stable well or, in other words, only 30% of the molecules have remained in the metastable well and will contribute to further relaxation. The latter are those molecules with the smallest tunnel splitting values within the distribution. After this, we turn on a transverse field, $H_T=0.4$ T, applied at an arbitrary angle, ϕ, with respect to the crystallographic axes of the sample. Then we sweep the longitudinal field to a high positive value, crossing the resonances again. We repeated this procedure for different orientations of the transverse field from 0 to 360 degrees.

The MQT probability of resonance $k=6$ is shown as a function of ϕ in Fig. 24. The results show the same fourfold symmetry pattern with maxima placed at the same positions as those in the experiment shown in Fig. 22. As these two experiments study the relaxation of two different parts of the distribution of tunnel splittings (low and high ends of the distribution), we can conclude that the fourfold symmetry of MQT is a property of a significant fraction of the molecules within the crystal.

In principle, the four fourfold rotation pattern is consistent with a fourth order transverse anisotropy term, $C(S_+^4 + S_-^4)$, in the spin-Hamiltonian (see Fig. 4b). For positive C, the four maxima generated by this term should be at $\phi_{max} = 45^\circ, 135^\circ, 225^\circ$ and 315°. There is a difference

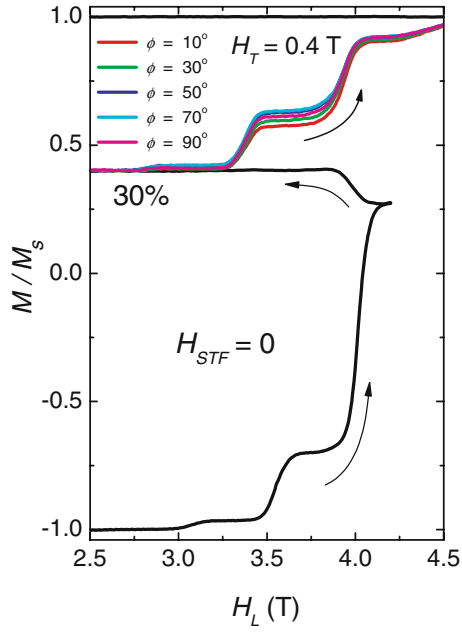

Fig. 23. (Color on-line) Selection of 30% of the molecules with the smallest tunnel splittings within the distribution. Starting at $M = -M_S$, the longitudinal field is swept from 0 to 4.2 T, then back to 0 in the absence of a transverse field (black line). After this procedure, only those molecules that have not relaxed (30%) remain in the metastable well. A transverse field of 0.4 T is then applied at an angle ϕ, and the longitudinal field is swept again to a high positive value. The process is repeated for different ϕ angles (lines with different colors).

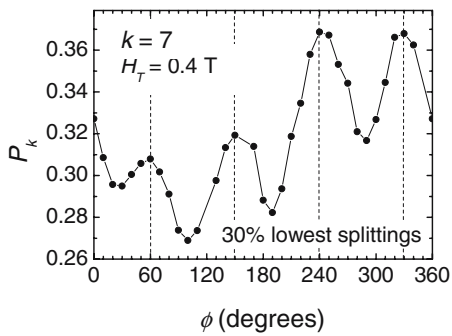

Fig. 24. MQT probability for resonance $k = 7$ versus the orientation of the applied transverse field, $H_T = 0.4$ T, relative to one of the faces of the crystal. A previous selection process was used to study only 30% of the molecules with the smallest tunnel splitting values within the distribution. The results were extracted from longitudinal magnetic field relaxation curves recorded at a constant sweep rate, $\alpha = 6.6 \times 10^{-3}$ T/s.

of 15 degrees between these values and those observed in our experiments, $\phi_{max} = 60^\circ, 150^\circ, 240^\circ$ and 330°. This is due to the misalignment, $\varphi = 12^\circ$, between the hard anisotropy axis of the molecules and one of the faces of the crystal, which we use as the origin of our ϕ rotation. There still is a difference of 3 degrees that is within the accuracy with which we orient the crystal (± 5 degrees). However, the value of $C \sim 3 \times 10^{-5}$ K cannot explain the difference between the maximal and minimal magnitudes of the measured MQT probability. The observed normalized changes, $(P_{max} - P_{min})/P_{max}$, in the experiment with 100% of the molecules contributing to the relaxation are ~ 0.9 for $k = 5$ and ~ 0.6 for $k = 6$ (see Fig. 22). Whereas, with this value of C, we expect this change to be within the noise of the measurement.

In order to determine whether this symmetry is intrinsic to the Mn_{12}-ac molecules and its origin, we have carried out experiments designed to select different parts of the distribution by using transverse fields in the selection process. Note that, in the previous experiment, we selected the SMMs with the smallest tunnel splittings in the absence of transverse fields. Now, we use a selection transverse field (STF), H_{STF}, applied at an angle, ϕ_{STF}, during the preparation of the initial state of the system. In this case, those molecules with the medium anisotropy axis aligned with the STF have larger tunnel splitting values (larger relaxation probability) and can be selected for further study.

The measurements with this selection process are shown in Fig. 25. First we apply a high longitudinal field to saturate the magnetization of the system and sweep the field back to zero, having at the end a magnetization, $M = -M_s$. Then we turn on a selection transverse field, $H_{STF} = 0.6$ T, applied at the angle $\phi_{STF} = 60^\circ$, where one of the four maxima were observed in the experiments carried out with the whole sample, and we sweep the longitudinal field at a constant rate to a positive value and sweep back to zero. The value of this field is chosen depending on how much relaxation we want in the selection process: for a selection of 50% of the biggest splittings, we sweep the field up to 3.2 T allowing the system to relax in resonances $k = 5$ and 6; for a selection of the 10% of the biggest splittings, we only allow the system to relax in resonance $k = 5$. The final states of the magnetization are $M = 0$ and $M = -0.8 M_s$, respectively. After the selection process we sweep the longitudinal field down to -5.5 T at a constant rate, $\alpha = 6.6 \times 10^{-3}$ T/s, in the presence of a transverse field, $H_T = 0.3$ T, applied at difference angles ϕ with respect to one of the faces of the crystal. We repeated this procedure for different angles ϕ from 0 to 360 degrees. In a separate experiment, we repeated the selection of 50% of the molecules with the largest splittings within the distribution by applying

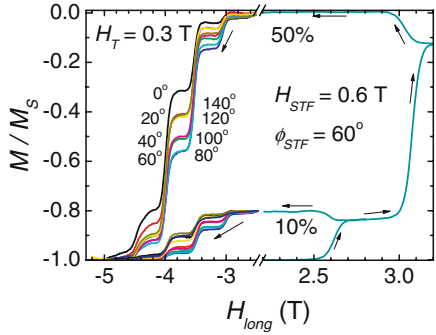

Fig. 25. (Color on-line) Selection processes carried out by sweeping a positive longitudinal field across resonances $k=5$ and $k=6$, in the presence of a selection transverse field, $H_{\mathrm{STF}}=0.6\,\mathrm{T}$, applied at a selection angle $\phi_{\mathrm{STF}}=60^{\circ}$. Both 10% and 50% of the molecules with the largest tunnel splitting values were selected in separate processes for this experiment. These populations were then studied on the negative side of the longitudinal field hysteresis curve, in the presence of a transverse field, $H_{\mathrm{T}}=0.3\mathrm{T}$, applied at different angles ϕ from 0 to 360 degrees.

a selection transverse field, H_{STF}, along the angle in which a complementary maximum was observed, $\phi_{\mathrm{STF}}=150^{\circ}$.

The results are shown in Fig. 26. In all selections the MQT probability shows a twofold rotation pattern with maxima spaced by 180 degrees. For the selection in which H_{STF} is applied along $\phi_{\mathrm{STF}}=60^{\circ}$, the two maxima are at $\phi_{\mathrm{max},1}=60^{\circ}$ and $\phi_{\mathrm{max},2}=240^{\circ}$, for both fractions of molecules selected (10% and 50%). Moreover, when the selection field is applied along the position of a complementary fourfold maximum, $\phi_{\mathrm{STF}}=150^{\circ}$, the twofold maxima, $\phi_{\mathrm{max},1}=150^{\circ}$ and $\phi_{\mathrm{max},2}=330^{\circ}$, are displaced by 90 degrees with respect to the previous case.

The observation of a twofold rotation pattern in the MQT probability is clear evidence of a second order transverse anisotropy lower than that imposed by the site symmetry of the molecule (four-fold). This is in excellent agreement with the solvent disorder model proposed by Cornia et al.[16] where there is an expectation of equal populations of molecules with opposite signs of the second order anisotropy. A considerable increase of the change of probability between maxima and minima is also observed as the fraction of molecules with highest tunnel splitting values becomes smaller, indicating the fact that the molecules with largest splitting values have bigger values of the second order anisotropy.

In Sec. 2, we stated that incommensurate anisotropy terms would considerably modify the magnetic response of the molecules to the orientation of a transverse magnetic field, depending on the angle of misalignment,

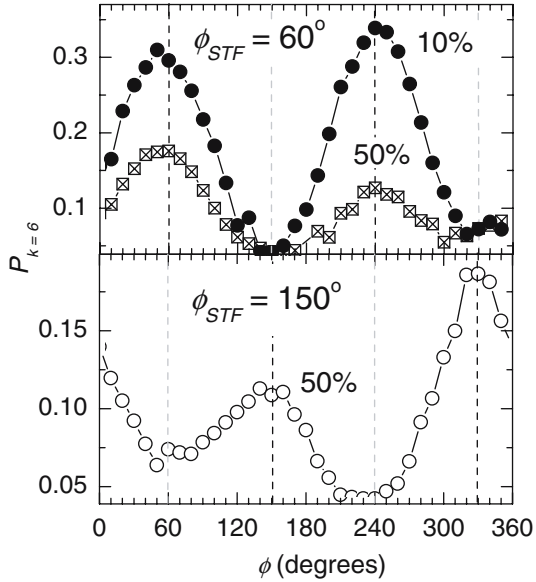

Fig. 26. Behavior of the MQT probability versus the orientation of a transverse field, $H_T = 0.3$ T. The molecules which relax were previously selected from the tunnel splitting distribution using a selection transverse field, H_{STF}, applied along the directions where the two complementary maxima where observed in the experiments on the whole sample (Fig. 24), i.e. $\phi_{STF} = 60°$ (upper figure, for both 10% and 50% of the largest splittings in the distribution), and $\phi_{STF} = 150°$(lower figure, for 50% of the largest splittings).

β, between both anisotropies (see Eqs. (5) and (6) and Fig. 5). The symmetry of the MQT probability expected from this model depends on several parameters like the resonance number, k, and/or the misalignment angle, β. It turns out from this model that for $|E| < 30$ mK (bigger than the maximum E value expected from the solvent disorder model) the symmetry of the MQT probability mainly depends on the angle of misalignment, β, going from fourfold for small β values to twofold for big β values. Taking a given E value, the transition between fourfold to twofold maxima patterns as a function of β depends on the resonance number k. For example, for resonance $k = 0$ (Fig. 8a), the fourfold maxima pattern is observed for every misalignment value, where a slight twofold modulation is due to the second order anisotropy. For bigger resonances (i.e. $k = 6$), the transition between these two MQT probability symmetries is cleaner (see Fig. 9). For misalignment angles, $|\beta| < 20°$, the MQT probability shows fourfold symmetry modulated by the second order anisotropy. However, for angles $|\beta| > 20°$, the MQT probability symmetry is twofold.

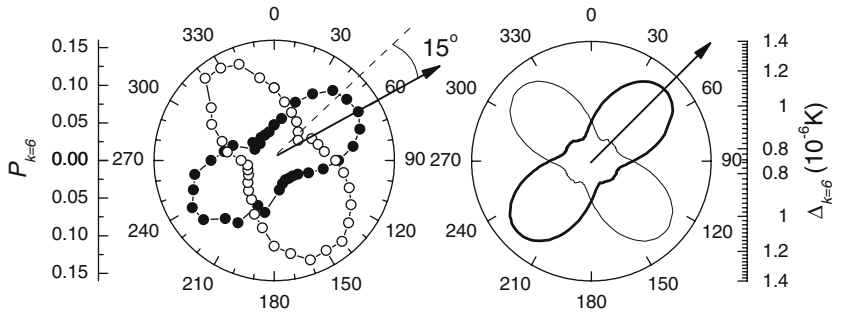

Fig. 27. *Left:* Experimentally determined angle dependence of the MQT probability for resonance $k=6$ for the two complementary directions of the transverse selection field. The one-fold contribution arising from the misalignment angles θ and σ has been corrected for clarity. *Right:* Calculated tunnel splitting for resonance $k=6$, $\Delta_{k=6}$, for $\beta=-30^\circ$ and opposite signs of E; the calculations assume the same values of H_T, D, E and C as those in Fig. 9.

Consequently, the observation of twofold symmetry in our experiments shows that the angle of misalignment between both anisotropy terms is greater than 20 degrees. In Sec. 4, we will present high frequency EPR experiments that show that the angle of this misalignment is $\beta=-30^\circ$. In Fig. 27 we show a comparison between the experimental observation of resonance $k=6$ for both transverse selection fields with 50% of the biggest splittings (left polar plot) and the calculated splitting (right polar plot) corresponding to resonance $k=6$ and $\beta=-30^\circ$ with opposite signs of $|E|=3$ mK. The difference of $\sim$15 degrees between the experimental results and the calculations is also shown in this figure. As we said before, this difference is due to the fact that we measure the angle ϕ with respect to one of the faces of the crystal while the transverse magnetic axes of the molecules are rotated from the faces of the crystal by $\sim$12 degrees.

An estimation of the values of E needed to explain the experimental observations of the oscillation of the MQT probability presented in this subsection are: (a) $E\sim 0.5$ mK for the result corresponding to the 30% of the smallest splittings of the distribution (Fig. 24), (b) $E\sim 2.5$ mK for the result with the whole distribution (Fig. 22, upper curve) and with 50% of the biggest splitting in the selection with $H_{STF}=60^\circ$ and 50° (Fig. 26), and (c) $E\sim 10$ mK for the result corresponding to 10% of the biggest splittings of the distribution (Fig. 26, solid circles). These values are in excellent agreement with the results obtained by high frequency EPR experiments (presented in Sec. 4) and by recent density functional theory calculations.[35] However, they are slightly larger than the values initially proposed in Ref. 16.

3.4. Berry Phase Measurements

The ability to select a subset of molecules with a narrow distribution of tunnel splittings and, for example, different signs of the second order transverse anisotropy allows us to study the behavior of the MQT relaxation as a function of a transverse field. As we anticipated in Sec. 2, quantum phase interference (Berry phase) would lead to zeros of the tunnel splittings (i.e. absence of magnetic relaxation) for several values of a transverse field applied along the hard anisotropy axis of the molecules, and we discussed how the pattern of the oscillations can be modified by the presence of two incommensurate transverse anisotropies.

For these experiments, we have used the same preparations of the initial states of the system as those shown in Fig. 25. These initial states correspond to a selection of 50% and 10% of the molecules having the larger tunnel splitting values within the distribution. The selection of both initial states is done by applying a selection transverse field, $H_{STF} = 0.6\,T$, at an angle $\phi_{STF} = 60^\circ$. As we have shown, this procedure mainly selects those molecules with one E-sign, as is observed in the twofold transverse field rotation pattern of the MQT probability of Fig. 26, with maxima at $\phi_{max} = 60^\circ,\ 240^\circ$ and minima at $\phi_{max} = 150^\circ, 330^\circ$. To study the behavior of the MQT probability as a function of the magnitude of the applied transverse field we apply a transverse field, H_T , along the direction of the first maximum, $\phi = 60^\circ$, after the selection process. We then sweep the longitudinal field at a constant rate to $-5.5\,T$, measuring the change of magnetization in each resonance crossing. We follow the same procedure for different values of the transverse field from $H_T = 0$ to $0.7\,T$. Moreover, we repeated the same measurement by applying the transverse field along the direction of the first minimum $\phi = 150^\circ$.[45] The results of the MQT probability for resonances $k = 5$, 6 and 7 are shown in Fig. 28. In the left graph of the figure are the results obtained with 50% of the molecules with the largest tunnel splitting values. In the right graph we show the results for 10% of the biggest splittings. The measurements with the transverse field applied along the first of the twofold maxima, $\phi = 60^\circ$, are represented by open symbols, while the solid symbols correspond to measurements with the transverse field applied along the first of the minima, $\phi = 150^\circ$.

There are several important aspects to this figure. (a) There is vertical shift between the curves corresponding to different directions of application of the transverse field. The shift is bigger in the case of the selection of the 10% of the biggest splittings within the distribution. This is consistent with the observations of Fig. 26, and supports the assumption of a distribution in the magnitude of the second order anisotropy. (b) MQT probability increases exponentially with the magnitude of the transverse

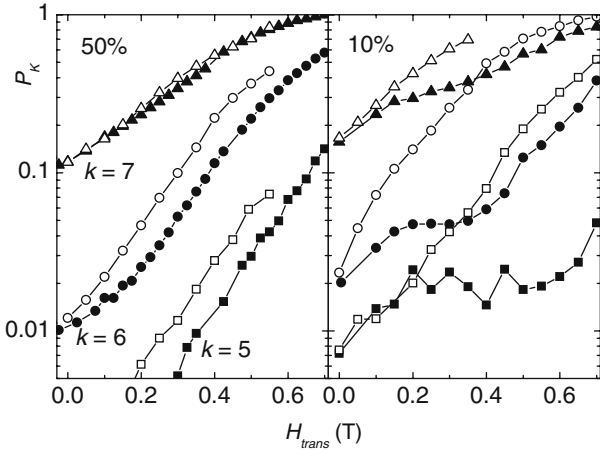

Fig. 28. MQT probability for resonances $k = 5, 6$ and 7 as a function of the magnitude of a transverse field applied along $\phi = 60^\circ$ (open symbols) and $\phi = 150^\circ$ (solid symbols). The initial state of the sample was prepared by selection of 50% (left) and 10% (right) of the molecules with the largest tunnel splitting values, using a selection transverse field, $H_{STF} = 0.6\,T$, applied along $\phi_{STF} = 60^\circ$. The two transverse field orientations correspond to the first maximum ($\phi = 60^\circ$) and minimum ($\phi = 150^\circ$) of the twofold rotation pattern.

field. This is expected from the exponential dependence of the LZ probability on the tunnel splitting shown in Eq. (8), and the power law dependence of the tunnel splitting on the magnitude of the transverse field (see Eq. (3)).[32] There are significant deviations from the exponential behavior in the right hand graphic for a transverse field applied along the first of the twofold minima, $\phi = 150^\circ$. The largest deviations are observed at field $H_p(k = 5) \sim 0.45\,T$, $H_p(k = 6) \sim 0.3\,T$ and $H_p(k = 7) \sim 0.35\,T$. This is reminiscent of the Berry phase observed in Fe_8.[33]

The results shown on the right graph of Fig. 28 can be compared with the calculations of the tunnel splitting versus the transverse field shown in Fig. 13 that were performed by taking into account two incommensurate anisotropy terms in the Hamiltonian (Eqs. (5) and (6)). In fact, the values, $E = 10 - 15\,mK$, used in these calculations were chosen according to the results shown in Fig. 28 and agree with the values extracted from high frequency EPR measurements (Sec. 4). The agreement between theory and experiments is very good and constitutes the first evidence of quantum interference phenomena in a SMM system with incommensurate transverse anisotropies.

3.5. Summary of Magnetic Relaxation Experiments

We have shown in this section that LZ magnetic relaxation experiments allow us to determine the complete distribution of tunnel splittings in Mn_{12}-ac. The results obtained through a multi-crossing LZ method show that a distribution of second order anisotropies with non-zero mode is required in order to explain our data, such as in the solvent disorder model proposed by Cornia et al.[16] LZ relaxation experiments carried out in the presence of a transverse field applied at arbitrary directions with respect to the crystallographic axes of the sample enabled studies of the symmetry of the MQT probability. We have shown that the MQT probability has a general fourfold rotation pattern as a function of the orientation of a transverse field. This is associated with equal populations of molecules with opposite signs of a second order transverse anisotropy. The LZ method allows the selection of a subset of molecules with different values of the tunnel splitting for further study. By applying a transverse field in the selection process, we can select a fraction of molecules in the sample with lower symmetry and with different signs of E. Using this selection procedure we have studied a small fraction of molecules with one sign of E and with the largest tunnel splitting values within the distribution. These show an unusual Berry phase phenomena for several transverse field values that does not lead to complete zeroes in the tunnel splitting. Our results on the symmetry of MQT can be explained in terms of incommensurate transverse anisotropies in the Hamiltonian that explain, among other things, why the observed Berry phase phenomena does not depend in any simple way on that expected from either anisotropy term alone.

4. HIGH FREQUENCY EPR EXPERIMENTS

High frequency (40–200 GHz) single crystal Electron Paramagnetic Resonance (EPR) measurements were carried out using a millimeter-wave vector network analyzer (MVNA) and a high sensitivity cavity perturbation technique; this instrumentation is described elsewhere.[46] Temperature control in the range from 2 K to room temperature was achieved using a variable-flow cryostat. The magnetic field was provided by a horizontal superconducting split-pair magnet with vertical access, enabling angle dependent studies ($< 0.1^\circ$ resolution) and approximate alignment of the single crystal.[27] In order to make accurate comparisons with the magnetization studies presented in the preceding sections, all data presented in this section were performed on a single deuterated crystal of Mn_{12}-ac (d-Mn_{12}-ac), having approximate dimensions $1 \times 0.3 \times 0.3\,mm^3$. This crystal was selected from a batch of samples which had previously been

removed from the mother liquor and stored for 1 year in a refrigerator (at 5° C) prior to the measurement. This particular batch was grown using standard methods,[41] albeit in a completely independent synthesis from the samples used for the magnetization measurements. The sample was separately cooled under vacuum from room temperature at 5 K/min in one of two orientations for field rotation in (i) the x–y plane, and (ii) a plane perpendicular to the x–y plane. In the former case, the sample was mounted on the side wall of a cylindrical TE011 cavity (center frequency $= 53.1$ GHz, $Q \sim 20,000$) with its easy axis parallel to the cavity axis such that the microwave field H_1 was aligned parallel to the sample's easy axis (and, therefore, perpendicular to the applied DC field). In the latter case, the sample was mounted on the end plate of the same cavity, and DC field rotation was carried out for angles close to the x–y plane (within 15°), with the microwave H_1 field again parallel to the sample's easy z-axis. Field sweeps were restricted to 6.6 T due to limitations of the split-pair magnet. As will become apparent, the data obtained for the d-Mn_{12}-ac are in qualitative agreement with earlier published results obtained for the hydrogenated Mn_{12}-ac.[19,27]

4.1. Magnetic Symmetry Measurements in the High-Field Limit

In the preceding sections, it has been shown how the Landau–Zener method may be applied to SMMs in order to determine very weak transverse terms in Eq. (1). Moreover, the Landau–Zener method allows one to select molecules, based on the tunneling rates of the different species. Subsequently, by performing angle dependent studies on each sub-species, one can deduce the underlying symmetries of the dominant tunneling matrix elements. While this method is extremely powerful, it is evident from the discussion in Sec. 2.3 that, for systems with multiple sources of transverse anisotropy (intrinsic and extrinsic), deconvolution of the different contributions to the tunnel splittings can be problematic, i.e. in Figs. 6–9 it is seen that competing E and C terms results in a competition between the two-fold and four-fold symmetries of these interactions. The reason for this competition is that, at low-fields, the E and C terms operate in different high orders of perturbation theory, thereby resulting in a complicated interaction between the two perturbations.

At first sight, it is not obvious how EPR experiments, conducted in the GHz frequency range, could shed new light on the nature of transverse interactions which manifest themselves as miniscule tunnel splittings of order 10^4 Hz at low-fields. However, the so-called "tunnel-splittings" are measured by the Landau-Zener method at low field wherein the transverse terms operate in very high orders of perturbation theory within an m_z

basis (see Eq. (3)), where the quantization axis is defined by the global easy-axis of the crystal. For high magnetic fields applied in the transverse direction, such a picture is no longer valid due to the conflicting symmetries imposed by the crystal field and the applied field. Herein lies the beauty of the high-field EPR technique. By applying a sufficiently strong transverse field, one can reach a limit in which the appropriate basis of spin states is defined by a quantization axis parallel to the applied field, i.e. the x-direction. In such a limit, transverse zero-field interactions operate in zeroth-order. Consequently, their effects may be rather strong. As an illustration of this point, consider the simplest zero-field Hamiltonian:

$$\mathcal{H} = -DS_z^2 + E(S_x^2 - S_y^2) - g\mu_B H_x S_x, \tag{15}$$

Making a substitution for S_z^2 in terms of $(S_x^2 + S_y^2)$, one obtains:

$$\mathcal{H} = \frac{1}{2}(D+3E)S_x^2 + \frac{1}{2}(D-E)(S_y^2 - S_z^2) - g\mu_B H_x S_x, \tag{16}$$

which can be re-written as:

$$\mathcal{H} = \frac{1}{2}(D+3E)S_x^2 - g\mu_B H_x S_x, + \mathcal{H}'_{\mathcal{T}}, \tag{17}$$

This equation is diagonal in S_x, and has the same form as Eq. (15). Therefore, to lowest order, the high-field eigenvalues will be given by:

$$\epsilon(m_x) \approx \frac{1}{2}(D+3E)m_x^2 - g\mu_B H_x m_x, \tag{18}$$

Similar arguments hold for higher order transverse terms. Thus, the transverse high-field EPR spectra provide perhaps the most direct means of measuring these transverse terms. Indeed, this represents one of the more illustrative examples of the importance of high-field EPR as a spectroscopic tool for studying quantum magnetism. Not only does the effect of the zero-field transverse terms shift to zeroth order, but the symmetry of such interactions is also preserved. This is best illustrated using the same example as above, with the field applied along the y-axis instead of the x-axis. In this case, Eq. (15) may be re-written:

$$\mathcal{H} = \frac{1}{2}(D-3E)S_y^2 - g\mu_B H_y S_y + \mathcal{H}''_{\mathcal{T}}, \tag{19}$$

giving

$$\epsilon(m_y) \approx \frac{1}{2}(D-3E)m_y^2 - g\mu_B H_y m_y, \tag{20}$$

Thus, from Eqs. (18) and (20), it is apparent that the influence of the rombic (E) term changes sign upon rotating the applied field from

the x-axis of the E-tensor to the y-axis. This two-fold behavior is not unexpected; indeed, it is obtained also from the exact diagonalization calculations shown in Figs. 6–8, which correspond to the high-field/frequency limit discussed here. However, unlike lower-field calculations, the 2nd and 4th order interactions decouple completely at high-fields, as do other transverse interactions. Thus, one may consider their effects completely independent. This point is illustrated in Fig. 8, where it can be seen that the effect of an intrinsic fourth-order anisotropy is to produce a ground- to-first-excited-state splitting ($\Delta_{k=0}$) which oscillates as a function of the field orientation within the hard/medium plane, with a periodicity of 90°. The disorder-induced rhombic anisotropy, meanwhile, has no effect on this four-fold behavior. It simply causes a two-fold modulation of the tunnel splitting, which superimposes onto the four-fold behavior caused by the fourth-order interaction. Because of the complete independence of these effects, one can in principle determine any misalignment, β, between the hard axes associated with the second and fourth order transverse anisotropies, as illustrated in Fig. 8.

In order to make direct comparisons with other spectroscopic studies (e.g. neutron[12] and EPR[7,13,16]) we re-write the Hamiltonian of Eq. (1) in the following form:

$$\mathcal{H} = D'\left[S_z^2 - \frac{1}{2}S(S+1)\right] + E\hat{O}_2^{2'} + B_4^0\hat{O}_4^0 + B_4^4\hat{O}_4^4 + \mathcal{H}_Z \tag{21}$$

where $\mathcal{H} = \mu_B \vec{H} \cdot \overleftrightarrow{g} \cdot \vec{S}$ is the Zeeman term due to the applied magnetic field, $E\hat{O}_2^{2'}$ is the first term in Eq. (5), and $\hat{O}_B^A$ are the Steven's operators, of order B in the spin operators and possess A-fold symmetry (i.e. $\hat{O}_4^4 \equiv \frac{1}{2}(S_+^4 - S_-^4)$). The uniaxial parameter D' is not exactly the same as the D parameter in Eq. (1) [or Eqs. (15)–(20)]. This is due to the occurrence of an S_z^2 term in the $\hat{O}_4^4$ Steven's operator, i.e. the presence of a significant fourth-order axial anisotropy has the effect of renormalizing the quadratic m-dependence of the barrier.[48,49]

Figure 29 displays the microwave absorption obtained for different field orientations within the hard ($x - y$) plane of the sample; the temperature was 15 K and the frequency was 51.3 GHz in every case. The peaks in absorption correspond to EPR. The data were obtained at 7.5° intervals, where the angle ϕ refers to the field orientation relative to one of the flat edges of the square cross section of the sample. The resonances have been labeled according to the scheme described in Ref. 27. For fields applied approximately parallel to the hard plane, only α-resonances are observed (β-resonances appear for field rotation away from the hard plane, see below). The highest field peak, $\alpha 8$, corresponds to an excitation between levels which evolve from the $m_z = \pm 9$ zero-field doublet. The transition

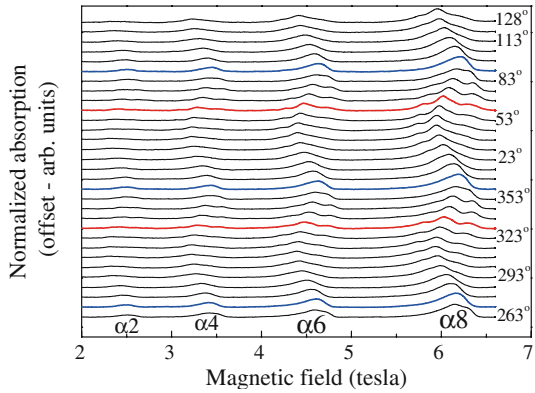

Fig. 29. (Color on-line) Microwave absorption obtained for different field orientations within the hard (xy-) plane of the sample; the temperature was 15 K and the frequency was 51.3 GHz in every case. The peaks in absorption correspond to EPR. The data were obtained at 7.5° intervals, where the angle ϕ refers to the field orientation relative to one of the flat edges of the square cross section of the sample. The resonances have been labeled according to the scheme described in Ref. 27. The red traces correspond to field orientations approximately parallel to the hard/medium axes of the E tensor, i.e. orientations corresponding to the maximum splitting of the low and high field shoulders. The blue traces correspond to orientations of the hard axes of the B_4^4 tensor.

from the ground state, $m_z = \pm 10$ ($k = 0$ resonance), is not observed within the available field range for these experiments; at 51 GHz, its expected position is at $H_T \sim 9$ T. For a detailed discussion of the resonance labeling scheme, as well as the temperature, frequency, field and field orientation dependence of the EPR spectra for Mn_{12}-ac, refer to Ref. 27.

Immediately apparent from Fig. 29 is a four-fold variation in the positions of each cluster of resonances ($\alpha 8$, $\alpha 6$, etc.). Note that each of the resonances exhibit fine structures, which also depend on the field orientation ϕ; these are related to the disorder in the crystal, which we discuss further below. The four-fold shifts are due to the intrinsic fourth-order transverse anisotropy $B_4^4 \hat{O}_4^4$, as has previously been established for h-Mn_{12}-ac.[19] Figure 30 shows a color contour plot of the absorption intensity versus magnetic field strength and the azimuthal angle ϕ. Superimposed on the absorption maxima are two kinds of fit to the ϕ-dependence of each peak. The solid blue curves were obtained simply by fitting the positions of the central peaks in Fig. 29 with pure sine functions having four-fold periodicity. The fits represented by horizontal bars, meanwhile, were obtained by exact diagonalization of the Hamiltonian matrix, assuming accepted values for the zero-field parameters D' and

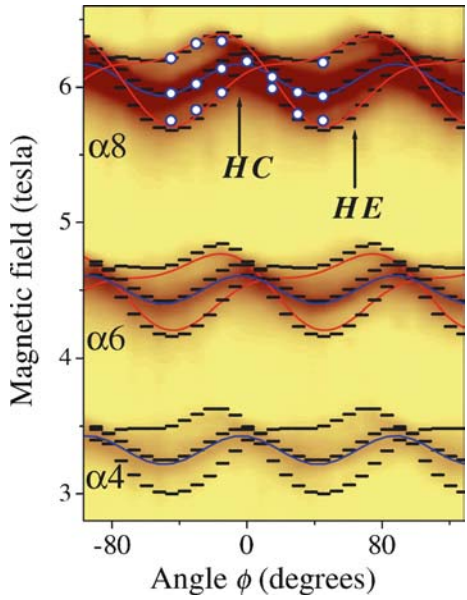

Fig. 30. (Color on-line) Color contour plot of the absorption intensity (see Fig. 29) versus magnetic field strength and the azimuthal angle ϕ; the darker shades correspond to stronger absorption. Superimposed on the absorption maxima are fits to the ϕ-dependence of the central positions of each peak (solid blue lines), as well as fits to the positions of the shoulders (solid red lines). The horizontal bars are fits to Eq. (21) (see main text for explanation). The approximate orientations of the hard axes corresponding to the E (HE) and B_4^4 (HC) tensors are indicated. The open circles represent recent data points obtained for h-Mn_{12}-ac.[47]

$B_4^0(D' = -0.455\,\mathrm{cm}^{-1}$ and $B_4^0 = 2\times10^{-5}\,\mathrm{cm}^{-1})$. The fourth-order transverse parameter $B_4^4 = 3.2\times10^{-5}\,\mathrm{cm}^{-1}$ is the only unknown parameter in the fit. D' and B_4^0 were verified independently from easy axis measurements, and all peak positions are consistent with a single value of B_4^4. We note that this value is in precise agreement with that found for h-Mn_{12}-ac, as is to be expected for this fourth-order interaction which is related to the intrinsic symmetry of the $Mn_{12}O_{12}$ molecule. From the maxima and minima in the peak position shifts induced by the $B_4^4\hat{O}_4^4$ term, we estimate that the hard and medium directions of this intrinsic crystal field interaction are oriented at $\phi_{HC} = -4.5^\circ \pm 5^\circ (+i90^\circ)$ and $\phi_{MC} = 41.5^\circ \pm 5^\circ (+i90^\circ)$ relative to the square edges of a typical single crystal sample.

Next we turn to the angle-dependent fine structures which are very apparent in the ranges $\phi = 300^\circ$–330° and $\phi = 30^\circ$–60° in Fig. 29. The first point to note is the fact that we see shoulders on both the high and low-field sides of the main peaks in these angle ranges. This contrasts the

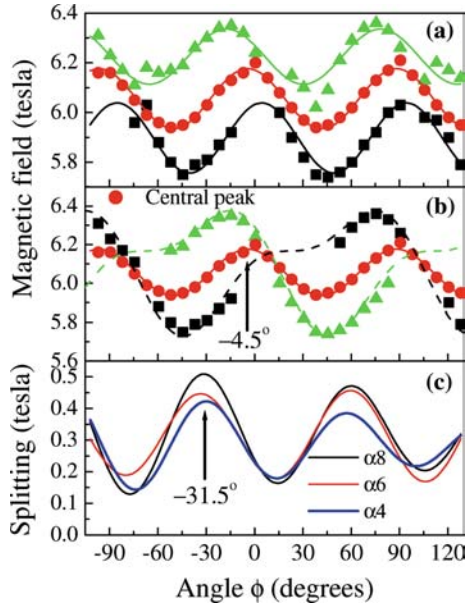

Fig. 31. (Color on-line) a) Hard-plane angle (ϕ) dependence of the splitting of the high and low-field shoulders, for the $\alpha 8$ peak. This figure may be compared with Fig. 2 of Ref. 19, which displays similar data for the h-Mn_{12}-ac complex. In (a), the positions of the low- (black) and high-field (green) shoulders on $\alpha 8$ have been separately fit with sine functions. The difference between these fits is displayed in (c), together with similar curves generated by the same procedure for peaks $\alpha 6$ and $\alpha 4$. The splittings plotted in (c) are a measure of the shifts caused by the disorder-induced rhombic term for the low-symmetry Cornia variants[16] (see also Fig. 8); all curves are in agreement ($\pm 2^\circ$) as to the orientation of the hard/medium two-fold directions. In (b), the data in (a) are plotted in such a fashion as to illustrate the real two-fold nature of the angle dependence of the high- and low-field shoulders. The approximate orientation ($\phi = -4.5^\circ$) of one of the hard four-fold axes (HC) is indicated in (b), and the approximate orientation ($\phi = -31.5^\circ$) of one of the hard/medium two-fold axes (HE) is indicated in (c).

situation found from our earlier studies of h-Mn_{12}-ac,[19] where only high-field shoulders were observed. We comment on these differences at the end of this section. We first discuss the origin of the angle dependence of the shoulders, which are very apparent in the ranges $\phi = 300^\circ$–330° and $\phi = 30^\circ$–60° in Fig. 29; a more in-depth discussion can be found in Refs. 19, 27. The high- and low-field shoulders are due to the $n = 1$ and $n = 3$ Mn_{12}-ac hydrogen-bonding variants in Cornia's solvent disorder model.[16] These variants, which comprise roughly 50% of the total molecules, are thought to possess a significant rhombic anisotropy due to the reduced symmetry of the surrounding hydrogen bonded acetic acid solvent molecules. The

second-order operator, $\hat{O}_2^2$, associated with the rhombic distortion gives rise to two-fold behavior, as was clearly demonstrated from the magnetic measurements in the previous section of this paper. It is important to recognize that the disorder is discrete, since the acetic acid can only bond at four positions on the Mn_{12} molecule. Thus, one expects only two hard directions associated with the $n = 1$ and $n = 3$ low symmetry variants, which are separated by 90°. In EPR, the $\hat{O}_2^2$ operator causes shifts in the peak positions. When the applied transverse field is parallel to one of the hard axes, it is obviously perpendicular to the other, which causes shifts in the EPR intensity to both the low- and high-field sides of the central peaks, hence the shoulders. When the field is applied in between these two directions, the EPR intensity due to the low-symmetry variants collapses into the central portion of the peak, hence the disappearance of the shoulders every 90° (see Figs. 29 and 30). In actual fact, this apparent four-fold behavior reflects the two-fold nature of the rhombic distortion caused by the hydrogen bonding acetic acid molecules, with the EPR intensity for a given variant shifting from the low (high) to the high (low) field side of the main peak every 90°, i.e. the periodicity is actually 180°. This two-fold behavior is then superimposed on the intrinsic four-fold periodicity, as can be seen in Fig. 31.

An important point to note from the hard-plane rotation data is the phase shift between the four-fold modulation of the central peak position (blue curves in Fig. 30) and the two-fold shifts of the low and high field shoulders (red curves in Fig. 30). Indeed, this is one of the main points of this article. As discussed in Sec. 2.3, this difference indicates a $\sim 27° \pm 3°$ misalignment of the $\hat{O}_2^2$ and $\hat{O}_4^4$ tensors, as was originally suspected for h-Mn_{12}-ac.[18,19] The present study provides further support for this finding, thereby illustrating the remarkable differences between the global and local symmetries of Mn_{12}-ac.

In order to make quantitative comparisons between the disorder-induced effects in h-Mn_{12}-ac and d-Mn_{12}-ac, we performed a single fit to each of the peaks in Fig. 30 via exact diagonalization of the Hamiltonian matrix [Eq. (21)]. This fit is represented by the horizontal bars in Fig. 30. Our procedure obviously takes into account the misalignments of the $\hat{O}_2^2$ and $\hat{O}_4^4$ tensors, as described in Sec. 2.3. Thus, the employed Hamiltonian is subtly different from the standard form used by most spectroscopists, which may explain slight differences in the obtained Hamiltonian parameters. The only free parameters in the fit were then the E and B_4^4 coefficients (corresponding to the $\hat{O}_2^2$ and $\hat{O}_4^4$ tensors), for which we obtained the values $\pm 0.014(2)\,\mathrm{cm}^{-1}$ and $\pm 3.2(5) \times 10^{-5}\,\mathrm{cm}^{-1}$ respectively. The E value is significantly larger than the one obtained in earlier experiments

(Ref. 19.) We attribute some of this difference to the modified Hamiltonian used in our more recent fits, which takes into account the misalignments of the $\hat{O}_2^2$ and $\hat{O}_4^4$ tensors. However, much of the difference appears to be real. The larger E-value found from the present study is somewhat surprising. However, as will be seen below, more recent measurements on a very fresh h-Mn_{12}-ac sample are in excellent agreement with the value of $\pm 0.014(2)\,cm^{-1}$ found from this study (open blue circles in Fig. 30). Thus, the difference is likely related to sample quality and/or solvent loss. A tell-tale sign of the higher sample quality is the observation of both high- and low-field shoulders on the main EPR peaks. In contrast, only high-field shoulders were seen in the earlier experiments on h-Mn_{12}-ac.[19,27] In fact, the absence of a low-field shoulder is discussed at some length in Ref. 27, where it is shown that this peak is unresolved from the broad low-field tail associated with the central portion of the peak. The reason for the asymmetry between the high and low-field shoulder is related to easy axis tilting caused by the solvent disorder (discussed in the next sub-section). Although both shoulders are seen in the present study, a clear asymmetry can be seen from the data in Fig. 29. We suspect that the samples used in the earlier experiments may have suffered significant solvent loss, either upon cooling from room temperature under high vacuum, or simply as a result of being stored in air for more than 1 year prior to the measurements. Indeed, variations in the D-strain measured in different Mn_{12}-ac samples has previously been reported by us.[21] Increased D-strain leads to broader EPR lines, thus probably explaining why the shoulders are clearly resolved in the present investigation, but not in Refs. 19, 27. Without two well resolved shoulders, it is likely that the E-strain was under-estimated in Ref. 19, or it could simply be that the E-strain is weaker in samples that suffer significant solvent loss. Based on more recent experience working with SMMs containing considerably more volatile solvents, we have recently developed sample handling procedures which minimize solvent loss, e.g. encapsulating samples in oil prior to cooling under atmospheric helium gas. The differences between the present measurements and those reported in Refs. 19, 27 highlight the importance of sample handling. Indeed, it is likely that Mn_{12}-ac samples prepared by different groups, and studied by different techniques, exhibit significant differences in their solvent content, resulting in subtly different conclusions concerning the quantum dynamics. Solvent loss probably also provides an explanation for the widths of the distributions of tunnel splittings found in the magnetic relaxation experiments described in Sec. 3. For this reason, it will be advantageous to prepare Mn_{12} SMMs which do not exhibit such a dramatic dependence on solvent content.

4.2. Easy-Axis Tilting

In this section, we briefly present the results of measurements for field rotations away from the hard plane in order to illustrate the presence of a small distribution of tilts of the easy axes of the d-Mn_{12}-ac molecules. In the following figures, the polar angle θ represents the angle between the applied DC magnetic field and the global easy axis of the crystal, i.e. $\theta = 90^\circ$ indicates the hard/medium-plane direction. Field rotation was performed in a plane approximately parallel to one of the large flat surfaces of the needle-shaped crystal (i.e. $\phi = 0$, or 90°, etc.). A more extensive discussion of the analysis and interpretation of the results of similar experiments for the h-Mn_{12}-ac complex have been published elsewhere.[27] Consequently, we present only data for d-Mn_{12}-ac in this article, and discuss the implications without including detailed simulations, which will be published elsewhere.[47]

Figure 32 shows a series of absorption spectra obtained at 0.2° intervals over the range from $\theta = 90^\circ$ to 97°. Again, the peaks in absorption correspond to EPR, and the labeling is discussed in Ref. 27. The quality of the data is noticeably poorer than the data in Fig. 29, and is due to the positioning of the sample at a different location in the cavity, where the geometry of the electromagnetic fields are not quite optimal for EPR. Figure 33 displays (a) a gray scale contour map and (b) a 3D plot representing the same data shown in Fig. 32 (the darker colored regions correspond to stronger EPR absorption), albeit for a wider range of angles (up to $\theta = 105^\circ$). As discussed at great length in Ref. 27, the transverse-field EPR spectra for Mn_{12}-ac exhibit unusual selection rules for frequencies below 90 GHz: two series of resonances are separately observed (labeled α and β) as the magnetic field is tilted away from the hard plane. These selection rules are extremely sensitive to the field orientation for angles close to the hard plane. Thus, deviations from the behavior predicted by the giant spin model (Eq. (1)) provide evidence for tilts of the molecules.

51.3 GHz simulations of the EPR spectra for an idealized Mn_{12}-ac sample are displayed in Fig. 34 – both a color contour map for the full $\theta = 90^\circ$ to 105° range (Fig. 34a), and a 3D view for the $\theta = 90^\circ$ to 97° range (Fig. 34b). These 15 K simulations were generated using the accepted Hamiltonian parameters given above. A Gaussian line shape was employed with a line width typical for a single solvent-disorder variant in Cornia's model (see Ref. 27). While this line shape/width is clearly quite different from the experimental data, which is complicated by the contributions of several Mn_{12}-ac variants, we note that the choice of line width/shape does not affect the following analysis. The simulations indicate a range of about 1.6° (from 91.8° to 93.4°) over which the EPR inten-

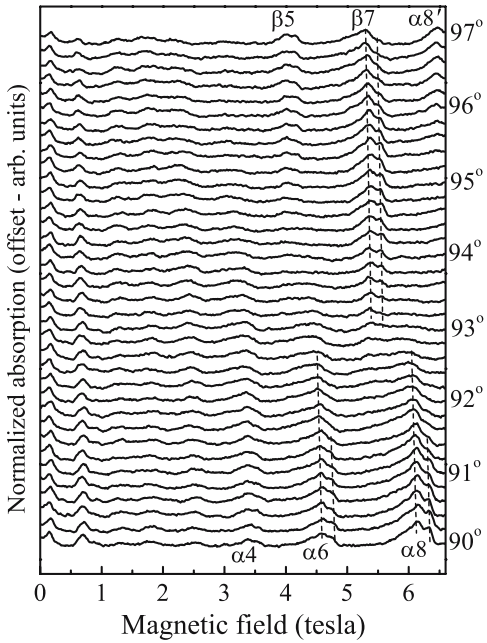

Fig. 32. (Color on-line) Microwave absorption spectra obtained at 0.2° intervals over the range from $\theta = 90°$ to 97° ($\phi \sim 5°$); the temperature was 1.5 K and the frequency was 51.3 GHz in every case, and the traces are offset for clarity. The peaks in absorption correspond to EPR, and the labeling is discussed in Ref. 27. See main text for discussion of the data.

sity associated with both the $\alpha 8$ and $\beta 7$ transitions is negligible. Thus, for a perfect crystal, without any disorder, one should expect a similar behavior in the actual EPR spectra. However, careful inspection of Figs. 32 and 33 indicates a significant overlap of the $\alpha 8$ and $\beta 7$ peaks in the 92° to 93° range. These two facts point to a spread in the orientations of the magnetic axes of the molecules, with a cut-off of at ~1.3° away from the global directions, i.e. we predict that, on average, the magnetic easy axes of the low-symmetry (disordered) molecules are tilted away from the crystallographic z-axis, and that the distribution extends roughly 1.3°. Once again, a very similar behavior has been observed for h-Mn_{12}-ac in Ref. 27, albeit that the distribution extends to ~1.7°. We note that the h-Mn_{12}-ac experiments were conducted using a rotating cavity[50] to higher magnetic field, where the experimental deviation from the simulation is even more pronounced. Thus, easy axis tilting appears to be a general feature in Mn_{12}-ac and, as discussed earlier in this article, this likely provides

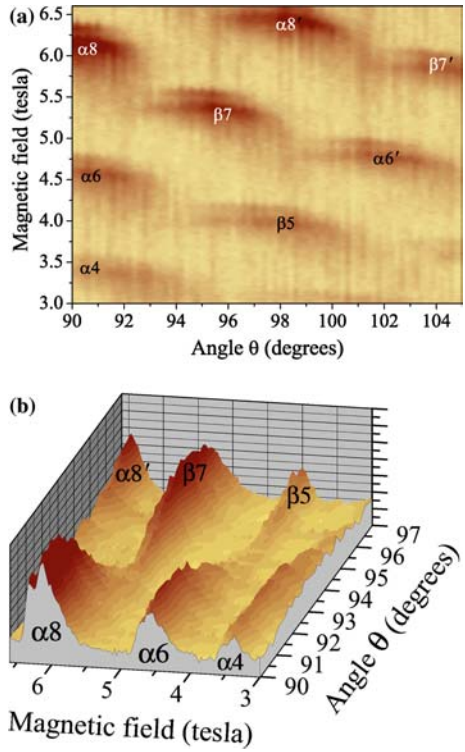

Fig. 33. (Color on-line) (a) A color contour map and (b) a 3D color surface plot representing the same data shown in Fig. 32 (the darker colored regions correspond to stronger EPR absorption). We plot the data in this manner for direct comparison with simulations shown in Fig. 34. The significant overlap of the α and β resonances suggests tilting of the molecules. See main text and Ref. 27 for discussion.

an explanation for the lack of selection rules in the magnetization steps observed from hysteresis experiments. The slightly broader tilt distribution for h-Mn_{12}-ac may be related to the increased solvent loss.

Finally, we comment on the correlation between the disorder-induced rhombic anisotropy and the easy axis tilting. It has been shown by Park *et al.*,[35] that the magnetic anisotropy tensor absolutely determines the orientations of the principal magnetic axes. In other words, one expects the effects of the solvent disorder to be accompanied by local easy-axis tilting. This was also pointed out by Cornia *et al.*[16] in their *x*-ray analysis of Mn_{12}-ac. We have subsequently shown this to be the case from EPR studies of h-Mn12-ac,[27] where it was shown that the high-field fine structures in the transverse EPR spectra displayed a different angle dependence

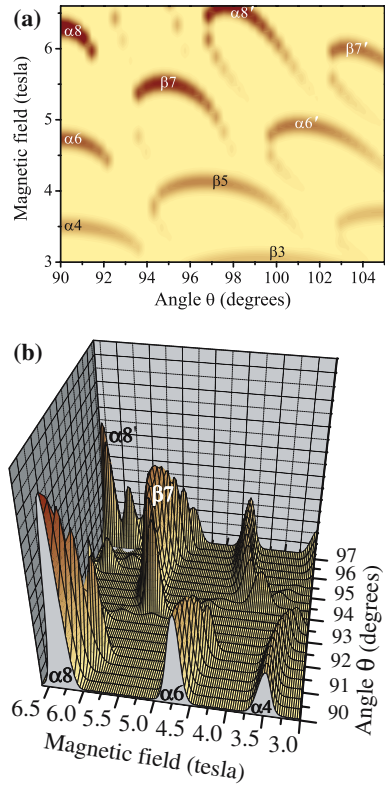

Fig. 34. (Color on-line) (a) A color contour map and (b) a 3D color surface plot representing simulations of the data in Fig. 33, assuming that all molecules are aligned, i.e. no tilting. The simulations were generated using the Hamiltonian parameters given in the text, and the temperature and frequency are 15 K and 51.3 GHz, respectively.

compared to the main peaks. These findings suggested that each solvent disorder variant has a distinct angle dependence and, therefore, a distinct tilting behavior, i.e. the tilting and the anisotropy are correlated. This is again apparent for d-Mn_{12}-ac from Fig. 33a, where the shoulders are visible as narrow horizontal streaks on the high field sides of each of the main peaks. It is quite evident that the narrow streaks (i.e. the shoulders) span a narrower angle range compared to the main peaks. In fact, the high field shoulders on the $\alpha 8$ and $\beta 7$ peaks exhibit a considerable range where neither is observed. Indeed, this range corresponds almost exactly to the 1.6° found from the simulations (Fig. 34). It is important to note that this local tilting of the magnetic axes (caused by local symmetry lowering), is quite

different from physical tilting of the molecules caused e.g. by strains in the sample.

Comparisons between Figs. 32, 33 and 34 indicate that the angle dependence of the high-field shoulders agrees very well with the simulations. The reason for these differences between the main peaks and the shoulders is explained in Ref. 27 as being due to discrete easy axis tilting, wherein the tilting is confined to two orthogonal planes defined by the hard and medium directions of the associated disorder-induced $\hat{O}_2^2(E)$ zero-field tensor. Essentially, the high-field shoulders on the EPR peaks are due to molecules which are tilted in a plane which is approximately perpendicular to the plane of rotation of the applied magnetic field. Consequently, the tilts due to these molecules do not project onto the field rotation plane, i.e. the experiment is insensitive to tilts in this direction. Meanwhile, the low-field tail of the EPR peaks is due to molecules which tilt in the orthogonal plane. For these molecules, the tilts have a maximum projection on to the field rotation plane, i.e. the experiment is maximally sensitive to tilts in this direction. The present studies support the findings of the original study for h-Mn_{12}-ac,[27] providing further confirmation for the discrete tilting idea.

5. CONCLUSIONS

In summary, these experiments provide a comprehensive understanding of the factors that influence the symmetry of MQT in Mn_{12}-ac, the first and most widely studied SMM. Interestingly, the reason so much attention has focused on Mn_{12} has been the high global symmetry of single crystals, as most known SMMs have lower site symmetry. The data presented here show that disorder lowers the symmetry locally and leads to an intricate interaction between transverse anisotropy terms: the first associated with disorder and the second intrinsic to an "ideal" Mn_{12}-molecule. While at first sight a nuisance, these complexities have been interesting from many perspectives. From experiment, they have been a challenge to understand and characterize, and have required combining unique advanced and sensitive magnetic characterization techniques that have been developed by the authors over many years. In particular, this research involved combining single crystal high-frequency and high-field EPR and low-temperature magnetometry, both with arbitrarily directed applied magnetic fields. The results obtained by magnetic measurements of MQT have had implications for EPR studies and vice-versa. From a theoretical perspective, given a structural model of the molecule and solvent environment, density functional theory has been able to capture many of the features observed in these experiments, including the magnitudes and form of the transverse magnetic anisotropies and the easy axis tilts.[35] This

includes the angle between the 2nd order and 4th order transverse anisotropies, which has been central to understanding the combined data set, as well as the easy axis tilts. This research thus represents an important milestone in our understanding of the factors that influence MQT in SMMs.

ACKNOWLEDGMENTS

This research was supported by NSF (Grant Nos. DMR-0103290, 0114142, 0239481 and 0315609). S. H. acknowledges Research Corporation for financial support.

REFERENCES

1. L. van Hemmen and A. Suto, *Europhys. Lett.* **1**, 481 (1986); L. van Hemmen and A. Suto, *Physica* **B141**, 37 (1986); M. Enz and R. Schilling, *J. Phys.* **C19**, 1765, L711 (1986); E. Chudnovsky and L. Gunther, *Phys. Rev. Lett.* **60**, 661 (1988).
2. J. Tejada, E. M. Chudnovsky, E. del Barco, and J. M. Hernandez, *Nanotechnology* **12**, 181 (2001); D. Loss, M. Leuenberger, and D. DiVincenzo, *Nature* **410**, 789 (2000).
3. J. R. Friedman, M. P. Sarachik, J. Tejada, and R. Ziolo, *Phys. Rev. Lett.* **76**, 3830 (1996).
4. J. M. Hernandez *et al., Europhys. Lett.* **35**, 301 (1996).
5. L. Thomas, F. Lionti, R. Ballou, D. Gatteschi, R. Sessoli, and B. Barbara, *Nature* (London) **383**, 145 (1996).
6. C. Sangregorio, T. Ohm, C. Paulsen, R. Sessoli, and D. Gatteschi, *Phys. Rev. Lett.* **78**, 4645 (1997).
7. A. L. Barra, D. Gatteschi, and R. Sessoli, *Phys. Rev.* B**56**, 8192 (1997).
8. J. A. A. J. Perenboom, J. S. Brooks, S. Hill, T. Hathaway, and N. S. Dalal, *Phys. Rev.* B**58**, 330 (1998).
9. K. M. Mertes *et al., Phys. Rev. Lett.* **87**, 227205 (2001).
10. J. M. Hernandez, F. Torres, J. Tejada, and E. Molins, *Phys. Rev.* B**66**, 161407 (2002).
11. L. Bokacheva, A. D. Kent, and M. A. Walters, *Phys. Rev. Lett.* **85**, 4803 (2000); A. D. Kent *et al., Europhys. Lett.* **49**, 521 (2000).
12. I. Mirebeau *et al., Phys. Rev. Lett.* **83**, 628 (1999).
13. S. Hill, J. A. A. Perenboom, N. S. Dalal, T. Hathaway, T. Stalcup, and J. S. Brooks, *Phys. Rev. Lett.* **80**, 2453 (1998).
14. E. M. Chudnovsky and D. A. Garanin, *Phys. Rev. Lett.* **87**, 187203 (2001).
15. E. M. Chudnovsky and D. A. Garanin, *Phys. Rev.* B**65**, 094423 (2002).
16. A. Cornia, R. Sessoli, L. Sorace, D. Gatteschi, A. L. Barra, *Phys. Rev. Lett.* **89**, 257201 (2002).
17. E. del Barco, A. D. Kent, E. M. Rumberger, D. N. Hendrickson and G. Christou, *Europhys. Lett.* **60**, 768 (2002).
18. E. del Barco, A. D. Kent, E. M. Rumberger, D. N. Hendrickson and G. Christou, *Phys. Rev. Lett.* **91**, 047203 (2003).
19. S. Hill, R. S. Edwards, S. I. Jones, N. S. Dalal, and J. M. North, *Phys. Rev. Lett.* **90**, 217204 (2003).
20. K. Park *et al., Phys. Rev.* B**65**, 014426 (2002).
21. S. Hill *et al., Phys. Rev.* B**65**, 224410 (2002).
22. R. Amigo *et al., Phys. Rev.* B**65**, 172403 (2001).
23. S. Maccagnano, R. Achey, E. Negusse, A. Lussier, M. M. Mola, S. Hill, and N. S. Dalal, *Polyhedron* **20**, 1441 (2001).
24. K. Park, M. A. Novotny, N. S. Dalal, S. Hill, and P. A. Rikvold, *J. Appl. Phys.* **91**, 7167 (2002).

25. B. Parks, J. Loomis, E. Rumberger, D. N. Hendrickson, and G. Christou, *Phys. Rev*. B**64**, 184426 (2001).
26. A. A. Mukhin *et al., Europhys. Lett*. **44**, 778 (1998).
27. S. Takahashi, R. S. Edwards, J. M. North, S. Hill and N. S. Dalal, *Phys. Rev*. B**70**, 094429 (2004).
28. E. del Barco, A. D. Kent, N. Chakov, G. Christou, and D. N. Hendrickson, *Phys. Rev*. B**69**, 020411(R) (2004).
29. T. Lis, *Acta Crystallogr*., Sect. B: *Struct. Crystallogr. Cryst. Chem*. **36**, 2042 (1980).
30. G. Christou, *et al., MRS Bull*. **25**, 66 (2000).
31. N. Regnault, Th. Jolicœur, R. Sessoli, D. Gatteschi and M. Verdaguer, *Phys. Rev*. B**66**, 054409 (2002).
32. D. Garanin and E. M. Chudnovsky, *Phys. Rev*. B**57**, 11102 (1997).
33. W. Wernsdorfer and R. Sessoli, *Science* **284**, 133 (1999).
34. C. Kirman, J. Lawrence, S. Hill, E-C. Yang, and D. N. Hendrickson, *J. Appl. Phys* **97**, 10M501 (2005).
35. K. Park, T. Baruah, N. Bernstein and M. R. Pederson, *Phys. Rev*. B **69**, 144426 (2004).
36. D. Loss, D. P. DiVincenzo and G. Grinstein, *Phys, Rev. Lett*. **69**, 3232 (1992).
37. A. Garg, *Europhys. Lett*. **22**, 205 (1993).
38. W. Wernsdorfer, M. Soler, G. Christou, and D. N. Hendrickson, *J. Appl. Phys*. **29**, 7164 (2002).
39. M. R. Pederson, J. Kortus, and S. N. Khanna, *J. Appl. Phys*. **91**, 7149 (2002).
40. C. S. Park and A. Garg, *Phys. Rev*. B**65**, 064411 (2002).
41. d-Mn_{12}-acetate was synthesized by following the standard procedure for preparing h-Mn_{12}- acetate, but using D_2O and deuterated acetic, CD_3COOD.
42. A. D. Kent, S. von Molnar, S. Gider, and D. D. Awschalom, *J. Appl. Phys*. **76**, 6656 (1994).
43. C. Zener, *Proc. R. Soc*. London A **137**, 696 (1932); S. Miyashita, *J. Phys. Soc. Jpn*. **64**, 3207 (1995); V. V. Dobrovitski and A. K. Zvezdin, *Europhys. Lett*. **38**, 377 (1997); L. Gunther *ibid*. **39**, 1 (1997); G. Rose and P. C. E. Stamp, *J. Low Temp. Phys*. **113**, 1153 (1998).
44. In the result presented in Ref. 18 the one-fold contribution of this measurement was displaced by 180 degrees. This corresponds to a mistake that was due to the fact that for this experiment we took $\phi = -180^\circ$ (that corresponds to negative orientation of one of the coils of the superconducting vector magnet) as the origin of rotation while for all the others the origin was $\phi = 0$ (positive orientation of the same coil) and we did not correct it in the data.
45. We studied the behavior of the MQT probability with a transverse field applied along the directions of a maximum and a minimum of the twofold MQT probability response because our initial interpretation of the results in Ref. 18 neglected the effect of incommensurate transverse anisotropies and we assumed that those were the directions of the hard and the medium anisotropy axes associated with $E(S_x^2 - S_y^2)$. As we explain in this article, these directions, in fact, correspond to medium anisotropy axes of the fourth order anisotropy term and none of them are along the hard anisotropy axes of the second order anisotropy term.
46. M. Mola, S. Hill, P. Goy, and M. Gross, *Rev. Sci. Inst*. **71**, 186 (2000).
47. S. Hill *et al*., Polyhedron (in press, 2005).
48. The $\hat{O}_4^0$ Stevens operator has the form $35\hat{S}_z^4 + [25 - 30S(S+1)]\hat{S}_z^2$. Thus, a finite B_4^0 term results in an additional quadratic contribution to the anisotropy barrier. Consequently, the axial crystal field parameters D (Eq. 1) and D' (Eq. 21) are inequivalent in situations where B (and, therefore, B_4^0) are finite; B and B_4^0 are inequivalent also. D and D', as well as B and B_4^0, also have opposite signs. The appropriate transformation between the two parameter sets are as follows: $D = (3275 \times B_4^0) - D'$ and $B = -35 \times B_4^0$.
49. M. R. Pederson, N. Bernstein, and J. Kortus, *Phys. Rev. Lett*. **89**, 097202 (2002).
50. S. Takahashi and S. Hill, *Rev. Sci. Inst*. **76**, 023114 (2005).